Ultimate Acceleration to Calculate the Global Climate Change: Atmosphere Issue

Huaiyang Cui

Department of Physics, Beihang University, Beijing, 102206, China

Email: hycui@buaa.edu.cn, hycui.blogspot.com

(September 1, 2022, submitted to viXra)

Abstract: In analogy with the ultimate speed c, there is an ultimate acceleration β, nobody's acceleration can exceed this limit β, in the solar system, β=2.961520e+10(m/s^2). Because this ultimate acceleration is a large number, any effect connecting to β will become easy to test, including quantum gravity tests. In this paper, an approach is put forward to connect the ultimate acceleration with quantum theory, as an application, this relativistic model gives out the sunspot cycle to be 10.38 years due to the ultimate acceleration. The same approach is applied to the Earth El Niño oscillation and global climate change cycle, calculating out the El Niño irregular period to be 8.5 years; calculating out the global climate change cycle to be 100.6 kiloyears which coincides with the Milankovitch cycle; the global temperature has increased about 0.8°C for the past century. In the atmosphere, the more serious the air pollution, the stronger the wind.

1. Introduction

In general, some quantum gravity proposals [1,2] are extremely hard to test in practice, as quantum gravitational effects are appreciable only at the Planck scale [3]. But ultimate acceleration gives another scheme to enhance the quantum gravity effects.

In 1843, German pharmacist H.S. Schwabe found that the growth and decline of sunspots had a period of about 10 years through his own observation records of sunspots for more than 20 years. In 1848, J.R. Wolf calculated the monthly sunspot relative number to 1749, thus affirming that the average cycle length of sunspot activity was 11.1 years. In 2019, there are 288 days without sunspots, and 40 consecutive days ahead. On December 25, 2019, two new sunspots appeared in the southern hemisphere of the sun, indicating the arrival of the 25th sunspot cycle, which is expected to reach its peak in July 2025. Although it is known that the cycle of sunspot activity is about 11 years, what drives this non-stop pattern is still a mystery.

Detailed estimates of temperature and carbon dioxide levels over the past 800000 years can be made from Antarctic ice samples. Within this time range, Earth's temperature has gone up and down, with glaciation and CO_2 levels [32]. Although broadly consistent with the Milankovitch hypothesis, a number of specific observations are not explained by the hypothesis.

In analogy with the ultimate speed c, there is an ultimate acceleration β, nobody's acceleration can exceed this limit β, in the solar system, β=2.961520e+10(m/s^2). Because this ultimate acceleration is a large number, any effect connecting to β will become easy to test, including quantum gravity tests. In this paper, an approach is put forward to connect the ultimate acceleration with quantum theory, as an application, this relativistic model gives out the sunspot cycle to be

10.38 years due to the ultimate acceleration. The same approach is applied to the Earth El Niño oscillation and global climate change cycle, calculating out the El Niño irregular period to be 8.5 years; calculating out the global climate change cycle to be 100.6 kiloyears which coincides with the Milankovitch cycle; the global temperature has increased about 0.8°C for the past century. In the atmosphere, the more serious the air pollution, the stronger the wind.

2. How to connect the ultimate acceleration with quantum theory

In the relativity, the speed of light c is an ultimate speed, nobody's speed can exceed this limit c. The relativistic velocity u of a particle in the coordinate system $(x_1,x_2,x_3,x_4=ict)$ satisfies

$$u_1^2 + u_2^2 + u_3^2 + u_4^2 = -c^2 \ . \tag{1}$$

No matter what particles (electrons, molecules, neutrons, quarks), their 4-vector velocities all have the same magnitude: $|u|=ic$. All particles gain **equality** because of the same magnitude of the 4-velocity u. The acceleration a of a particle is given by

$$a_1^2 + a_2^2 + a_3^2 = a^2; \quad (a_4 = 0; \quad \because x_4 = ict) \tag{2}$$

Assume that particles have an ultimate acceleration β as limit, no particle can exceed this acceleration limit β. Subtracting the both sides of the above equation by β^2, we have

$$a_1^2 + a_2^2 + a_3^2 - \beta^2 = a^2 - \beta^2; \qquad a_4 = 0 \tag{3}$$

It can be rewritten as

$$[a_1^2 + a_2^2 + a_3^2 + 0 + (i\beta)^2]\frac{1}{1 - a^2/\beta^2} = -\beta^2 \tag{4}$$

Now, the particle subjects to an acceleration whose five components are specified by

$$\alpha_1 = \frac{a_1}{\sqrt{1 - a^2/\beta^2}}; \quad \alpha_2 = \frac{a_2}{\sqrt{1 - a^2/\beta^2}};$$

$$\alpha_3 = \frac{a_3}{\sqrt{1 - a^2/\beta^2}}; \quad \alpha_4 = 0; \quad \alpha_5 = \frac{i\beta}{\sqrt{1 - a^2/\beta^2}}; \tag{5}$$

where α_5 is the newly defined acceleration in five dimensional space-time $(x_1,x_2,x_3,x_4=ict,x_5)$. Thus, we have

$$\alpha_1^2 + \alpha_2^2 + \alpha_3^2 + \alpha_4^2 + \alpha_5^2 = -\beta^2; \quad \alpha_4 = 0 \tag{6}$$

It means that the magnitude of the newly defined acceleration α for every particle takes the same value: $|\alpha|=i\beta$ (constant imaginary number), all particle accelerations gain **equality** for the sake of the same magnitude.

How to resolve the velocity u and acceleration α into x, y, and z components? In realistic world, a hand can rotate a ball moving around a circular path at constant speed v with constant centripetal acceleration a, as shown in Fig.1(a).
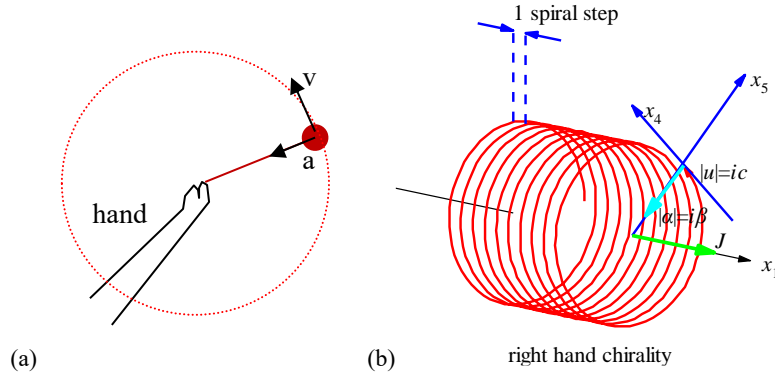
2

Fig.1 (a) A hand rotates a ball moving around a circular path at constant speed v with constant centripetal acceleration a. (b) The particle moves along the x_1 axis with the constant speed $|u|=ic$ in the u direction and constant centripetal force in the x_5 axis at the radius iR (imaginary number).

```
<Clet2020 Script>//[26]
double D[100],S[2000];int i,j,R,X,N;
int main(){R=50;X=50;N=600;D[0]=-50;D[1]=0;D[2]=0;D[3]=X;D[4]=0;D[5]=0;D[6]=-50;D[7]=R;D[8]=0;
D[9]=600;D[10]=10;D[11]=R;D[12]=0;D[13]=3645;
Lattice(SPIRAL,D,S);SetViewAngle(0,80,-50);DrawFrame(FRAME_NULL,1,0xffffff);
Draw("LINE,0,2,XYZ,0","-150,0,0,-50,0,0");Draw("ARROW,0,2,XYZ,10","50,0,0,150,0,0");
SetPen(2,0xff0000);Plot("POLYLINE,0,600,XYZ",S[9]);i=9+3*N-6;Draw("ARROW,0,2,XYZ,10",S[i]);
TextHang(S[i],S[i+1],S[i+2]," #if|u|=ic#t");TextHang(150,0,0," #ifx#sd1#t");SetPen(2,0x005fff);
Draw("LINE,1,2,XYZ,8","-50,0,50,-50,0,100");Draw("LINE,1,2,XYZ,8","-40,0,50,-40,0,100");
Draw("ARROW,0,2,XYZ,10","-80,0,100,-50,0,100");Draw("ARROW,0,2,XYZ,10","-10,0,100,-40,0,100");
TextHang(-50,0,110,"1 spiral step");i=9+3*N;S[i]=50;S[i+1]=10;S[i+2]=10;
Draw("ARROW,0,2,XYZ,10","50,0,0,50,80,80");TextHang(50,80,80," #ifx#sd5#t");
Draw("ARROW,0,2,XYZ,10","50,72,50,0,72);TextHang(50,0,72," #ifx#sd4#t");
SetPen(3,0x00ffff);Draw("ARROW,0,2,XYZ,15",S[i-3]);TextHang(S[i],S[i+1],S[i+2]," #if|α|=iβ#t");
SetPen(3,0x00ff00);Draw("ARROW,0,2,XYZ,15","50,0,0,120,0,0");TextHang(110,5,5," #ifJ#t");
TextHang(-60,0,-80," right hand chirality");}#v07=?>A
```

In analogy with the ball in a circular path, consider a particle in one dimensional motion along the x_1 axis at the speed v, in the Fig.1(b) it moves with the constant speed $|u|=ic$ almost along the x_4 axis and slightly along the x_1 axis, and the constant centripetal acceleration $|\alpha|=i\beta$ in the x_5 axis at the constant radius iR (imaginary number); the coordinate system $(x_1,x_4=ict,x_5=iR)$ establishes a cylinder coordinate system in which this particle moves spirally at the speed v along the x_1 axis. According to usual centripetal acceleration formula $a=v^2/r$, the acceleration in the x_4-x_5 plane is given by

$$a=\frac{v^2}{r} \quad \Rightarrow \quad i\beta=\frac{|u|^2}{iR}=-\frac{c^2}{iR}=i\frac{c^2}{R} \cdot \tag{7}$$

Therefore, the track of the particle in the cylinder coordinate system $(x_1,x_4=ict,x_5=iR)$ forms a shape, called as **acceleration-roll**. The faster the particle moves along the x_1 axis, the longer the spiral step is.

As like a steel spring that contains elastic wave, the track in the acceleration-roll in Fig.1(b) can be described by a wave function whose phase changes 2π for one spiral step. Apparently, this wave is the de Broglie's matter wave for electrons, protons or quarks, etc.

Theorem: the acceleration-roll bears the matter wave.

Proof: The wave function phase changes 2π for one spiral circumference $2\pi(iR)$, then a small displacement of the particle on the spiral track is $|u|d\tau=icd\tau$ in the 4-vector u direction, thus this wave phase along the spiral track is evaluated by

3

$$phase = \int_0^\tau \frac{2\pi}{2\pi(iR)} ic \, d\tau = \int_0^\tau \frac{c}{R} d\tau \quad . \tag{8}$$

Substituting the radius R into it, the wave function ψ is given by

$$\psi = \exp(-i \cdot phase) = \exp(-i\int_0^\tau \frac{c}{R} d\tau) = \exp(-i\frac{\beta}{c}\int_0^\tau d\tau) \quad . \tag{9}$$

In the theory of relativity, we known that the integral along $d\tau$ needs to transform into realistic line integral, that is

$$d\tau = -c^2 \frac{d\tau}{-c^2} = (u_1^2 + u_2^2 + u_3^2 + u_4^2)\frac{d\tau}{-c^2}$$
$$= (u_1 dx_1 + u_2 dx_2 + u_3 dx_3 + u_4 dx_4)\frac{1}{-c^2} \tag{10}$$

Therefore, the wave function ψ is evaluated by

$$\psi = \exp(-i\frac{\beta}{c}\int_0^\tau d\tau)$$
$$= \exp(i\frac{\beta}{c^3}\int_0^x (u_1 dx_1 + u_2 dx_2 + u_3 dx_3 + u_4 dx_4)) \tag{11}$$

This wave function may have different explanations, depending on the particle under investigation. If the β is replaced by the Planck constant, the wave function of electrons is given by

$$assume: \quad \beta = \frac{mc^3}{\hbar}$$
$$\psi = \exp(\frac{i}{\hbar}\int_0^x (mu_1 dx_1 + mu_2 dx_2 + mu_3 dx_3 + mu_4 dx_4)) \tag{12}$$

where $mu_4dx_4=-Edt$, it strongly suggests that the wave function is just the de Broglie's matter wave [4,5,6]. Proof is done.

In Fig.1(b), the acceleration-roll of particle moves with two distinctions: right-hand chirality and left-hand chirality. The direction of the angular momentum J would be slightly different from the x_1 due to spiral precession. It is easy to calculate the ultimate acceleration β , the radius R and the angular momentum J in the plane x_4-x_5 for a spiraling electron as

$$\beta = \frac{c^3 m}{\hbar} = 2.327421e+29 \, (M/s^2); \quad R = \frac{c^2}{\beta} = 3.861593e-13 \, (M) \tag{13}$$
$$J = \pm m|u|iR = \mp\hbar$$

```
<Clet2020 Script>//[26]
double beta,R,J,m,D[10];char str[200];
int main(){m=ME;beta=SPEEDC*SPEEDC*SPEEDC*m/PLANCKBAR;
R=SPEEDC*SPEEDC/beta;J=PLANCKBAR;Format(str,"beta=%e, #nR=%e, #nJ=%e",beta,R,J);
TextAt(50,50,str);ClipJob(APPEND,str);}#v07=#t
```

Considering another explanation to ψ for planets in the solar system, no Planck constant can be involved. But, in a many-body system with the total mass M, the data-analysis [28] tells us that the ultimate acceleration can be rewritten in terms of **Planck-constant-like constant** h as

4

$$assume: \quad \beta = \frac{c^3}{hM}$$

$$\psi = \exp(\frac{i}{hM}\int_0^x (u_1 dx_1 + u_2 dx_2 + u_3 dx_3 + u_4 dx_4)) \tag{14}$$

The constant h will be determined by experimental observations. This paper will show that this wave function is applicable to several many-body systems in the solar system, the wave function is called as the **acceleration-roll wave**.

Considering third explanation to ψ for atoms in cells and viruses. Typically, sound speed in water is $v=1450m/s$, according to $v=f\lambda$, the sound wavelength λ for frequency 1kHz ---1Mhz is 1.5m---1.45mm. In general, the sound wavelength is larger than cell size, because cell size is about 1 micro. Thus, almost all cells and viruses live in a smaller space which is not sensitive to the sound. The acceleration-roll can provide a kind of wave with a shorter wavelength and lower frequency for various cells and viruses beyond human-sensitive sound wave [28].

Of cause, there is an "ultimate distance" [28] from which the Hubble law can be derived out.

Tip: actually, ones cannot get to see the acceleration-roll of particle in the relativistic space-time ($x_1,x_2,x_3,x_4=ict$) ; only get to see it in the cylinder coordinate system ($x_1,x_4=ict,x_5=iR$).

3. How to determine the ultimate acceleration

In the Bohr's orbit model for planets or satellites, as shown in Fig.2, the circular quantization condition is given in terms of relativistic matter wave in gravity by

$$\left.\begin{array}{c} \frac{\beta}{c^3}\oint_L v_l dl = 2\pi n \\ v_l = \sqrt{\frac{GM}{r}} \end{array}\right\} \quad \Rightarrow \quad \sqrt{r} = \frac{c^3}{\beta\sqrt{GM}}n; \quad n=0,1,2,... \quad . \tag{15}$$
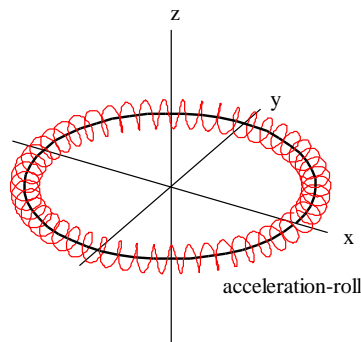

Fig.2   A planet 2D orbit around the sun, an acceleration-roll winding around the planet.

```
<Clet2020 Script>//[26]
int i,j,k; double r,rot,x,y,z,D[20],F[20],S[200]; int main(){SetViewAngle("temp0,theta60,phi-30");
DrawFrame(FRAME_LINE,1,0xafffaf);r=80;Spiral(); TextHang(r,-r,0,"acceleration-roll");
r=110;TextHang(r,0,0,"x");TextHang(0,r,0,"y");TextHang(0,0,r,"z");}
Spiral(){r=80;j=10;rot=j/r;k=2*PI/rot+1;
for(i=0;i<k;i+=1) {D[0]=x;D[1]=y;D[2]=z;D[6]=x;D[7]=y;D[8]=r;
x=r*cos(rot*i);y=r*sin(rot*i);z=0;if(i==0) continue;
SetPen(2,0x00);F[0]=D[0];F[1]=D[1];F[2]=x;F[3]=y;Draw("LINE,0,2,XY,",F);SetPen(1,0xff0000);
D[3]=x;D[4]=y;D[5]=z; D[9]=40;D[10]=10;D[11]=8;D[12]=0;D[13]=360;
Lattice(SPIRAL,D,S);Plot("POLYLINE,0,40,XYZ",S[9]);}
}#v07=?>A
```

The solar system, Jupiter's satellites, Saturn's satellites, Uranus' satellites, Neptune's satellites as five different many-body systems are investigated with the Bohr's orbit model. After fitting observational data as shown in Fig.3, their ultimate accelerations are obtained in Table 1. The predicted quantization-blue-lines in Fig.3(a), Fig.3(b), Fig.3(c), Fig.3(d) and Fig.3(e) agree well with experimental observations for those *inner constituent planets or satellites*.
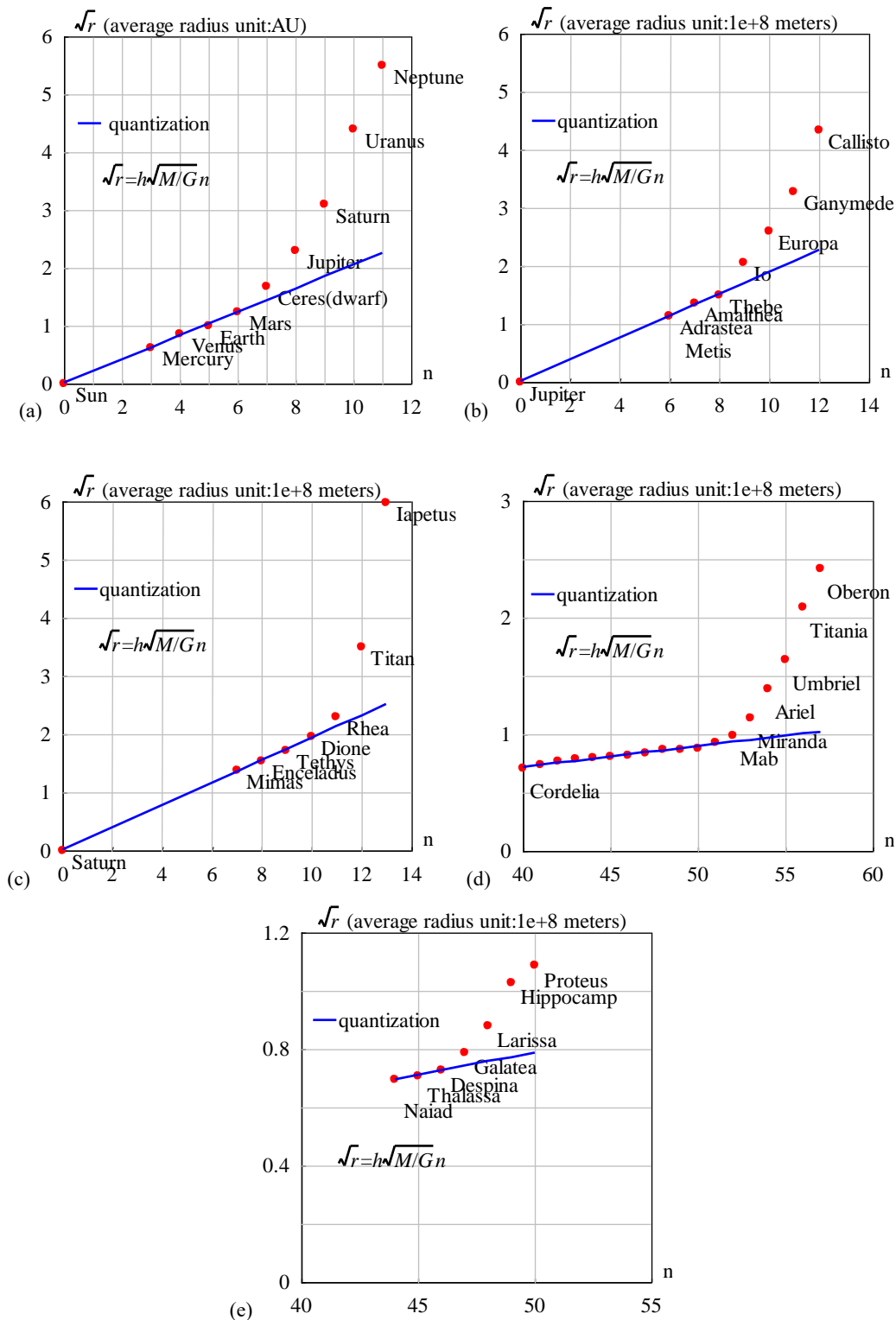

Fig.3 The orbital radii are quantized for inner constituents. (a) the solar system with h=4.574635e-16 (m^{2}s^{-1}kg^{-1}).

The relative error is less than 3.9%. (b) the Jupiter system with h=3.531903e-16 (m²s⁻¹kg⁻¹). Metis and Adrastea are assigned the same quantum number for their almost same radius. The relative error is less than 1.9%. (c) the Saturn system with h=6.610920e-16 (m²s⁻¹kg⁻¹). The relative error is less than 1.1%. (d) the Uranus system with h=1.567124e-16 (m²s⁻¹kg⁻¹). n=0 is assigned to the Uranus. The relative error is less than 2.5%. (e) the Neptune system with h=1.277170e-16 (m²s⁻¹kg⁻¹). n=0 is assigned to the Neptune. The relative error is less than 0.17%.

Table 1   Planck-constant-like constant h, N is constituent particle number with smaller orbital inclination.

system	N	M/M_{earth}	β (m/s2)	h (m2s-1kg-1)	Prediction
Solar planets	9	333000	2.961520e+10	4.574635e-16	Fig.3(a)
Jupiter' satellites	7	318	4.016793e+13	3.531903e-16	Fig.3(b)
Saturn's satellites	7	95	7.183397e+13	6.610920e-16	Fig.3(c)
Uranus' satellites	18	14.5	1.985382e+15	1.567124e-16	Fig.3(d)
Neptune 's satellites	7	17	2.077868e+15	1.277170e-16	Fig.3(e)

Besides every β, our interest shifts to the constant h in Table 1, which is defined as

$$h = \frac{c^3}{M\beta} \quad \Rightarrow \quad \sqrt{r} = h\sqrt{\frac{M}{G}}n \quad . \tag{16}$$

In a many-body system with the total mass M, a constituent particle has the mass m and moves at the speed v, it is easy to find that the wavelength of de Broglie's matter wave should be modified for planets and satellites as

$$\lambda_{de\_Broglie} = \frac{2\pi\hbar}{mv} \quad \Rightarrow \text{modify} \Rightarrow \quad \lambda = \frac{2\pi hM}{v} \quad . \tag{17}$$

where h is a **Planck-constant-like constant**. Usually the total mass M is approximately equal to the central-star's mass. It is found that this modified matter wave works for quantizing orbits correctly in Fig.3 [28,29]. The key point is that the various systems have almost same Planck-constant-like constant h in Table 1 with a mean value of 3.51e-16 m²s⁻¹kg⁻¹, at least have the same magnitude! The acceleration-roll wave is a generalized matter wave as a planetary scale wave.

In Fig.3(a), the blue straight line expresses the linear regression relation among the Sun, Mercury, Venus, Earth and Mars, their quantization parameters are hM=9.098031e+14(m²/s). The ultimate acceleration is fitted out to be β=2.961520e+10 (m/s²). Where, n=3,4,5,.. were assigned to solar planets, the sun was assigned a quantum number n=0 because the sun is in the **central state**.

4.   Optical model of the central state

The acceleration-roll wave as the relativistic matter wave generalized in gravity is given by

$$\psi = \exp(\frac{i}{hM}\int_0^x v_l dl); \quad \lambda = \frac{2\pi hM}{v_l} = \frac{2\pi c^3}{v_l\beta} \quad . \tag{18}$$

In a central state n=0, if the coherent length of the acceleration-roll wave is long enough, its head may overlap with its tail when the particle moves in a closed orbit in the space time, as shown in Fig.4, the interference of the acceleration-roll wave between its head and tail will occur in the overlapping zone. The overlapped wave is given by

$$\psi(r) = 1 + e^{i\delta} + e^{i2\delta} + ... + e^{i(N-1)\delta} = \frac{1 - \exp(iN\delta)}{1 - \exp(i\delta)}$$

$$\delta(r) = \frac{1}{hM} \oint_L (v_l) dl = \frac{2\pi\omega r^2}{hM} = \frac{2\pi\beta\omega r^2}{c^3} \tag{19}$$

where N is the overlapping number which is determined by the coherent length of the acceleration-roll wave, δ is the phase difference after one orbital motion, ω is the angular speed of the sun rotation. The above equation is a multi-slit interference formula in optics, for a larger N it is called as the Fabry-Perot interference formula.
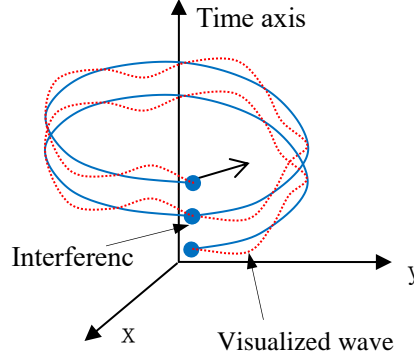
Fig.4   The head of the acceleration-roll wave may overlap with its tail.

The acceleration-roll wave function ψ needs a further explanation. In quantum mechanics, $|\psi|^2$ equals to the probability of finding an electron due to Max Burn's explanation; in astrophysics, $|\psi|^2$ equals to the probability of finding a nucleon (proton or neutron) *averagely in astronomic scale*, because all mass is mainly made of nucleons, we have

$$|\psi|^2 \propto nucleon\_density \tag{20}$$

It follows from the multi-slit interference formula that the interference intensity at maxima is proportional to N^2, that is

$$N^2 = \frac{|\psi(0)_{multi-wavelet}|^2}{|\psi(0)_{one-wavelet}|^2} \tag{21}$$

What matter plays the role of "one-wavelet" in the solar core or Earth core? We choose vapor above the sea on the earth surface as the "reference matter: one-wavelet". Thus, the overlapping number N is estimated by

$$N^2 = \frac{|\psi(0)_{multi-wavelet}|^2}{|\psi(0)_{one-wavelet}|^2} \approx \frac{core\_nucleon\_density_{r=0}}{vapor\_above\_sea\_density} \tag{22}$$

Although today there is not vapor on the solar surface, the solar core has a maximum density of 1.5e+5kg/m^3 [31], comparing to the vapor density 1.29 kg/m^3 on the earth, the solar overlapping number N is estimated as $N=341$. The Earth core density is 5.53e+3kg/m^3, the Earth's overlapping number N is estimated as $N=65$.

For the Sun, Earth and Mars, their central densities and their reference matter density are given in the Table 2. Thus, their overlapping numbers are estimated also in this table.

Table 2 Estimating the overlapping number N by comparing solid core to reference matter, regarding protons and neutrons as basis particles.

object	Solid core, density (kg/m^3)	Reference matter, density (kg/m^3)	Overlapping number N	β (m/s^2)
Sun	1.5e+5 (max.)	1.29 (vapor above the sea)	341	2.961520e+10
Earth	5530	1.29 (vapor above the sea)	65	1.377075e+14
Mars	3933.5	1.29 (vapor above the sea)	55	2.581555e+15
Jupiter	1326			4.016793e+13
Saturn	687			7.183397e+13
Uranus	1270			1.985382e+15
Neptune	1638			2.077868e+15
Alien-planet	5500	1.29(has water on the surface)	65	

Sun's rotation angular speed at the equator is known as $\omega=2\pi/(25.05*24*3600)$, unit s^{-1}. Its mass 1.9891e+30 (kg), radius 6.95e+8 (m), mean density 1408 (kg/m³), the solar core has a maximum density of 1.5e+5kg/m³ [31], the ultimate acceleration β=2.961520e+10 (m/s²), the constant hM= 9.100745e+14 (m²/s). According to the N=341, the matter distribution of the $|\psi|^2$ is calculated out in Fig.5, it agrees well with the general description of the sun's interior. The radius of the Sun is calculated out to be r=7e+8 (m) with a relative error 0.72% in the Fig.5, it indicates that the sun radius strongly depends on the sun self-rotation.
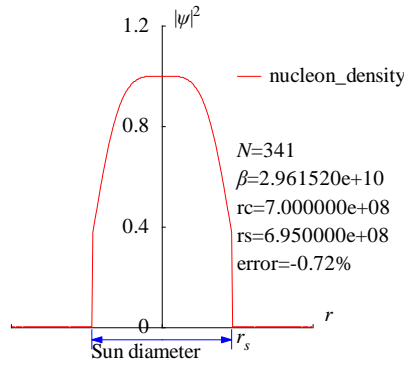

Fig.5 The matter distribution $|\psi|^2$ around the Sun has been calculated in radius direction.

```
<Clet2020 Script>//[26]
int i,j,k,m,n,N,nP[10];
double beta,H,B,M,r,r_unit,x,y,z,delta,D[1000],S[1000], a,b,rs,rc,rot,atm_height; char str[100];
main(){k=150;rs=6.95e8;rc=0;x=25.05;rot=2*PI/(x*24*3600);n=0; N=341;
beta=2.961520e10;H=SPEEDC*SPEEDC*SPEEDC/beta;M=1.9891E30; atm_height=2e6; r_unit=1E7;
b=PI/(2*PI*rot*rs*rs/H);
for(i=-k;i<k;i+=1) {r=abs(i)*r_unit;
if(r<rs+atm_height) delta=2*PI*rot*r*r/H; else delta=2*PI*sqrt(GRAVITYC*M*r)/H;//around the star
y=SumJob("SLIT_ADD,@N,@delta",D); y=y/(N*N);
S[n]=i;S[n+1]=y; if(i>0 && rc==0 && y<0.001) rc=r;D[n]=i;D[n+1]=z;n+=2;}
SetAxis(X_AXIS,-k,0,k,"#ifr; ; ; ;");SetAxis(Y_AXIS,0,0,1.2,"#if|ψ|#su2#t;0;0.4;0.8;1.2;");
DrawFrame(FRAME_SCALE,1,0xafffaf); z=100*(rs-rc)/rs;
SetPen(1,0xff0000);Polyline(k+k,S,k/2,1," nucleon_density"); SetPen(1,0x0000ff); //Polyline(k+k,D);
//Draw("LINE,0,2,XY,0","20,0.5,60,0.6");TextHang(60,0.6,0,"core");
r=rs/r_unit;y=-0.05;D[0]=-r;D[1]=y;D[2]=r;D[3]=y; Draw("ARROW,3,2,XY,10,100,10,10,",D);
Format(str,"#ifN#t=%d#n#ifβ#t=%e#nrc=%e#nrs=%e#nerror=%.2f%","N,beta,rc,rs,z);
TextHang(k/2,0.7,0,str);TextHang(r+5,y/2,0,"#ifr#sds#t");TextHang(-r,y+y,0,"Sun diameter");
}#v07=?>A
```

5. Earth central state and space debris distribution

Appling the acceleration-roll wav to the Moon, as illustrated in Fig.6(a), the Moon has been assigned a quantum number of $n=2$ in author's early study [28]. According to the quantum condition, the ultimate acceleration is fitted out to be $\beta=1.377075e+14$ (m/s^2) in the Earth system. Another consideration is to take the quasi-satellite's perigee into account, for the moon and 2004_GU9 etc., as shown in Fig.6(b), but this consideration requires further understanding to its five quasi-satellites [28].

(a) $H=1.956611e+11$ $B=0.000000e+00$ (b) $H=1.956611e+11$ $B=-5.221444e+10$
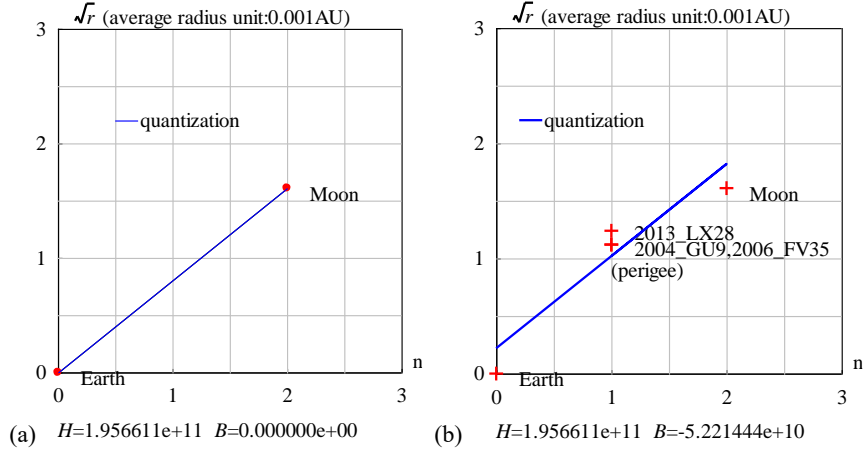
Fig.6   orbital quantization for moon and quasi-satellites to the Earth, $H=hM$.

```
<Clet2020 Script>//[26]
char str[200];int i,j,k,N,nP[10]; double x,y,z,M,r_unit,a,b,B,H,r_ave[20],dP[10],D[1000];
double orbit[10]={0,2.57,0,}; double e[10]={0, 0.0549,0,0,0,0,0,0,0,0,};
int qn[10]={0,2,3,4,5,6,7,8,9.,10,};
char Stars[100]={"Earth;Moon;"};
int main(){ N=2; M=5.97237E24; r_unit=1.495978707e8;
for(i=0;i<N;i+=1) {x=orbit[i];y=e[i]; z=x*(1+sqrt(1-y*y))/2;r_ave[i]=z;//average_radius
D[i+i]=qn[i];D[i+i+1]=sqrt(z); }
DataJob("REGRESSION,2",D,dP);b=dP[0];a=dP[1];
SetAxis(X_AXIS,0,0,3,"n;0;1;2;3;");
SetAxis(Y_AXIS,0,0,3," #if#rsr#t (average radius unit:0.001AU);0;1;2;3;");
DrawFrame(0x0166,1,0xafffaf); Polyline(N,D);
SetPen(2,0xff0000); Plot("OVALFILL,0,2,XY,3,3,",D);
for(i=0;i<N;i+=1) {nP[0]=TAKE;nP[1]=i;TextJob(nP,Stars,str);x=qn[i]+0.2;y=sqrt(orbit[i])-0.05;TextHang(x,y,0,str);}
x=GRAVITYC*M*r_unit;z=sqrt(x);H=z*a;B=-z*b;
TextAt(100,450,"#ifH#t=%e   #ifB#t=%e",H,B);
for(i=0;i<N;i+=1) {y=b+a*qn[i];D[i+i]=qn[i];D[i+i+1]=y;}
SetPen(1,0x0000ff);Polyline(N,D,0.5,2.2,"quantization");//check
}}#v07=?>A
```

Now let us talk about the central state of the earth, the earth's rotation angular speed is known as $\omega=2\pi/(24*3600)$, unit s^{-1}. Its mass 5.97237e+24(kg), radius 6.371e+6(m), core density 5530(kg/m^3), the ultimate acceleration $\beta=1.377075e+14$(m/s^2), the constant $hM=1.956611e+11$(m^2/s).

We have estimated that the wave overlapping number in the central state of the earth is $N=65$, the matter distribution $|\psi|^2$ in radius direction is calculated out as shown in Fig.7(a), where the self-rotation near its equator has the period of 24 hours:

$$\delta(r) = \frac{1}{hM} \oint_L (v_l) dl = \frac{2\pi r}{hM} \omega r = \frac{2\pi\beta\omega r^2}{c^3} \quad . \tag{23}$$

There is a central maximum of matter distribution at the earth heart, which gradually decreases to zero near the earth surface, then rises the secondary peaks and attenuates down off. The radius of the earth is calculated out to be r=6.4328e+6 (m) with a relative error 0.86% using the interference of its acceleration-roll wave. Space debris over the atmosphere has a complicated evolution [7,8], has itself speed

$$v_l = \sqrt{\frac{GM}{r}}; \quad \delta(r) = \frac{1}{hM} \oint_L (v_l)dl = \frac{\beta}{c^3} \oint_L (v_l)dl = \frac{2\pi\beta}{c^3}\sqrt{GMr} \quad . \qquad (24)$$

The secondary peaks over the atmosphere up to 2000km altitude is calculated out in Fig.7(b) which agrees well with the space debris observations [16]; the peak near 890 km altitude is due principally to the January 2007 intentional destruction of the Fengyun-1C weather spacecraft while the peak centered at approximately 770 km altitude was created by the February 2009 accidental collision of Iridium 33 (active) and Cosmos 2251 (derelict) communication spacecraft [16,18]. The observations based on the incoherent scattering radar EISCAT ESR located at 78°N in Jul. 2006 and in Oct. 2015 [21,22,23] are respectively shown in Fig.7(c) and (d). This prediction to secondary peaks also agrees well with other space debris observations [24,25].
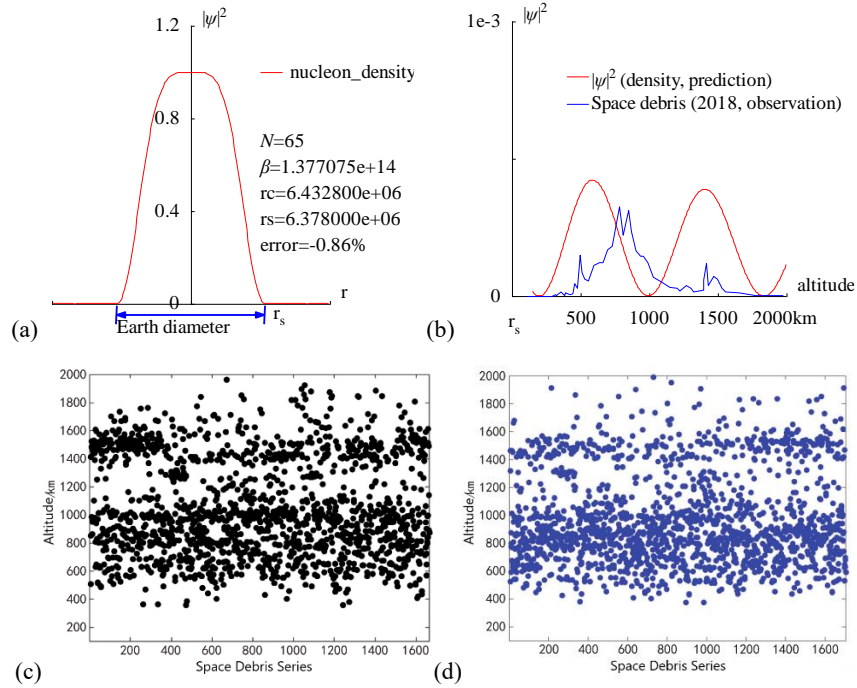

Fig.7 (a) The radius of the Earth is calculated out r=6.4328e+6 (m) with a relative error 0.86% by the interference of its acceleration-roll wave; (b) The prediction of the space debris distribution up to 2000km altitude; (c) The pace debris distribution in Jul. 2006, Joint observation based on the incoherent scattering radar EISCAT ESR located at 78°N [21]; (d) The space debris distribution in Oct. 2015, Joint observation based on the incoherent scattering radar EISCAT ESR located at 78°N [21].

```
<Clet2020 Script>//[26]
int i,j,k,m,n,N,nP[10];
double H,B,M,v_r,r,AU,r_unit,x,y,z,delta,D[10],S[1000];
double rs,rc,rot,a,b,atm_height,beta; char str[100];
main(){k=80;rs=6.378e6;rc=0;atm_height=1.5e5;n=0; N=65;
beta=1.377075e14;H=SPEEDC*SPEEDC*SPEEDC/beta;
M=5.97237e24;AU=1.496E11;r_unit=1e-6*AU;
rot=2*PI/(24*60*60);//angular speed of the Earth
for(i=-k;i<k;i+=1) {r=abs(i)*r_unit;
if(r<rs+atm_height) v_r=rot*r*r; else v_r=sqrt(GRAVITYC*M*r);//around the Earth
delta=2*PI* v_r/H; y=SumJob("SLIT_ADD,@N,@delta",D); y=y/(N*N);
if(y>1) y=1; S[n]=i;S[n+1]=y; if(i>0 && rc==0 && y<0.001) rc=r;   n+=2;}
SetAxis(X_AXIS,-k,0,k,"r; ; ; ;");SetAxis(Y_AXIS,0,0,1.2,"#if|ψ|#su2#t;0;0.4;0.8;1.2;");
DrawFrame(FRAME_SCALE,1,0xafffaf); x=50;z=100*(rs-rc)/rs;
SetPen(1,0xff0000);Polyline(k+k,S,k/2,1," nucleon_density");
r=rs/r_unit;y=-0.05;D[0]=-r;D[1]=y;D[2]=r;D[3]=y;
SetPen(2,0x0000ff); Draw("ARROW,3,2,XY,10,100,10,10,",D);
Format(str,"#ifN#t=%d#n#ifβ#t=%e#nrc=%e#nrs=%e#nerror=%.2f%",N,beta,rc,rs,z);
TextHang(k/2,0.7,0,str);TextHang(r+5,y/2,0,"r#sds#t");TextHang(-r,y+y,0,"Earth diameter");
}#v07=?>A
```

6. Mars and Jovian planets

The Mars and its satellites are quantized very well by its ultimate acceleration β as shown in Fig.8(a). Now let us talk about the Mars in the central state with quantum number n=0, its ultimate acceleration is β=2.581555e+15(m/s^2) in the Mars system. We have estimated the Mars overlapping number N=55 in Table 2, the matter distribution $|\psi|^2$ around the Mars can been calculated out in radius direction as shown in Fig.8(b), where the self-rotation at equator has the period of 24 hours.

   The radius of the Mars is calculated out as r=1.6e+6 (m) with a relative error 52.79%, no further attempt was made to improve the calculation, because of limited knowledge about the Mars history. But one thing is certain, the Mars has frequently bombarded with smaller objects, in fact, consequently with the inclination of 25.2 degrees, so that its self-rotation is unstable or incorrect for its formation in a sense. At very beginning, the Mars self-rotation should have a period of 100 hours. Thanks to the Mars for safeguarding the Earth.
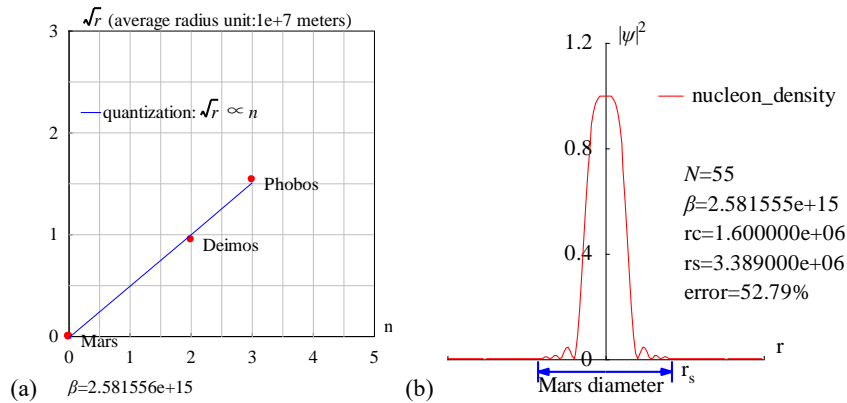

Fig.8   (a)Quantization of Mars and its satellites. (b)The matter distribution $|\psi|^2$ around the Mars has been calculated in radius direction.

```
Format(str,"#ifN#t=%d#n#ifβ#t=%e#nrc=%e#nrs=%e#nerror=%.2f%",N,beta,rc,rs,z);
TextHang(k/2,0.7,0,str);TextHang(r+5,y/2,0,"r#sds#t"); TextHang(-r,y+y,0,"Mars diameter");
}#v07=?>A
```

In order to extend the quantization rule to the Jovian planets (Jupiter, Saturn, Uranus and Neptune), it is necessary to further study the magnet-like components of gravity [28], the issue beyond the scope of this paper.

7. New aspect: coherent width and sunspot cycle

The **coherence length** of waves is usually mentioned but the **coherence width** of waves is rarely discussed in quantum mechanics, simply because the latter is not a matter for electrons, nucleon or photos, but it is a matter in astrophysics. The analysis of observation data tells us that on the planetary scale, the coherence width of the acceleration roll wave can be extended to 1000 kilometers or more, as illustrated in Fig.9(a), the overlap may even occur in the width direction, thereby bringing new aspects to wave interference.

In the solar convective zone, adjacent convective arrays form a top-layer flow, a middle-layer gas and a ground-layer flow, similar to the concept of **molecular current** in electromagnetism. Considering one convective ring at the equator as shown in Fig.9(b), there is an apparent velocity difference between the top-layer flow and the middle-layer gas, where their acceleration-roll waves are denoted respectively by
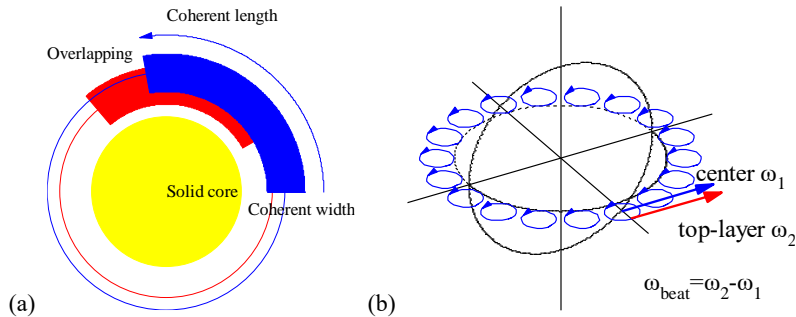

Fig.9   (a) Illustration of overlapping in coherent width direction. (b) Convective rings at the equator, the speed difference causes a beat frequency.

```
<Clet2020 Script>// [26]
int i, j, k, R,D[500];
main(){DrawFrame(FRAME_NULL,1,0xafffaf);
R=60; SetPen(1,0xffff00);
D[0]=-R; D[1]=-R; D[2]=R; D[3]=R; Draw("ELLIPSE,1,2,XY,0",D);
R=85;   k=15; SetPen(1,0xff0000);
D[0]=-R; D[1]=-R; D[2]=R; D[3]=R; Draw("ELLIPSE,0,2,XY,0",D);
D[0]=0; D[1]=0; D[2]=R-k; D[3]=0; D[4]=R+k;D[5]=0;
Draw("SECTOR,1,3,XY,15,30,130,0",D);
R=95; k=15; SetPen(1,0x00ff);
D[0]=-R; D[1]=-R; D[2]=R; D[3]=R; Draw("ELLIPSE,0,2,XY,0",D);
D[0]=0; D[1]=0; D[2]=R-k; D[3]=0; D[4]=R+k;D[5]=0;
Draw("SECTOR,1,3,XY,15,0,100,0",D);D[4]=R+k+k;
Draw("SECTOR,3,3,XY,15,0,100,0",D);
TextHang(0,0,0,"Solid core");TextHang(R-k-k,-k,0,"Coherent width");
TextHang(0,R+k+k+k,0,"Coherent length");TextHang(-R,R+k,0,"Overlapping");
}#v07=?>A


<Clet2020 Script>//Clet is a C compiler[26]
double beta,H,M,N,dP[20],D[2000],r,rs,rot,x,y,v1,v2,K1,K2,T1,T2,T,Lamda,V; int i,j,k;
int main(){beta=2.961520e10; H=SPEEDC*SPEEDC*SPEEDC/beta;
M=1.9891E30; rs=6.95e8;rot=2*PI/(25.05*24*3600);v1=rot*rs;K1=v1*v1/2;//T1=2*PI*H/K1;
v2=0.7346*sqrt(BOLTZMANN*5700/MP)+0.2485*sqrt(BOLTZMANN*5700/(MP+MP));
K2=v2*v2/2;T2=2*PI*H/(K2-K1);T=T2/24*3600*365.2422;
Lamda=2*PI*H/(v2-v1);V=Lamda/T2;
SetViewAngle("temp0,theta60,phi-60");
DrawFrame(FRAME_LINE,1,0xafffaf);Overlook("2,1,60", D);
```

```
//TextAt(10,10,"v1=%d, v2=%d, T=%.2f y, λ=%e, V=%d",v1,v2,T, Lamda,V);
SetPen(1,0x4f4fff); for(i=0;i<18;i+=1) {v1=i*2*PI/18; x=70*cos(v1);y=70*sin(v1);Ring();}
SetPen(2,0xff0000);Draw("ARROW,0,2,XYZ,15","80,0,0,80,60,0");
TextHang(100,20,0,"top-layer ω#sd2#t"); SetPen(2,0x0000ff);
Draw("ARROW,0,2,XYZ,15","70,0,0,70,60,0");
TextHang(50,60,0,"center ω#sd1#t");TextHang(140,-30,0," ω#sdbeat#t=ω#sd2#t-ω#sd1#t");
}
Ring(){ k=0;N=20; r=10;
for(j=0;j<N+2;j+=1) {k=j+j+j; v2=j*2*PI/N;
D[k]=x+r*cos(v2);D[k+1]=y+r*sin(v2); D[k+2]=0;}
Plot("POLYLINE,4,22,XYZ,8",D);}
#v07=?>A
```

$$\psi = \psi_{top} + C\psi_{middle}$$

$$\psi_{top} = \exp[\frac{i\beta}{c^3}\int_L (v_1 dl + \frac{-c^2}{\sqrt{1-v_1^2/c^2}}dt)]$$

$$\psi_{middle} = \exp[\frac{i\beta}{c^3}\int_L (v_2 dl + \frac{-c^2}{\sqrt{1-v_2^2/c^2}}dt)]$$

(25)

Their interference in the coherent width direction leads to a beat phenomenon

$$|\psi|^2 = |\psi_{top} + C\psi_{middle}|^2 = 1 + C^2 + 2C\cos[\frac{2\pi}{\lambda_{beat}}\int_L dl - \frac{2\pi}{T_{beat}}t]$$

$$\frac{2\pi}{T_{beat}} = \frac{\beta}{c^3}(\frac{c^2}{\sqrt{1-v_1^2/c^2}} - \frac{c^2}{\sqrt{1-v_2^2/c^2}}) \simeq \frac{\beta}{c^3}(\frac{v_1^2}{2} - \frac{v_2^2}{2})$$

(26)

$$\frac{2\pi}{\lambda_{beat}} = \frac{\beta}{c^3}(v_1 - v_2); \quad V = \frac{\lambda_{beat}}{T_{beat}} = \frac{1}{2}(v_1 + v_2)$$

Their speeds are calculated by

$$v_1 \approx 6200 \, (m/s) \quad (\approx \text{observed in Evershed flow})$$

$$v_2 = \omega r_{middle} = 2017 \, (m/s) \quad (\text{sun rotation});$$

(27)

Where, regarding the Evershed flow as the eruption of the top-layer flow, about 6km/s speed was reported [31]. Alternatively, the top-layer speed v_1 also can be calculated by thermodynamics, to be v_1=6244 (m/s) [28]. Thus, their beat period T_{beat} is calculated out to be a very remarkable value 10.38 (years), in agreement with the sunspot cycle value (say, mean 11years).

$$T_{beat} \simeq \frac{4\pi c^3}{\beta(v_1^2 - v_2^2)} = 10.38 \, (years) \; .$$

(28)

The relative error to the mean 11 years is 5.6% for the beat period calculation using the acceleration-roll waves. This beat phenomenon turns out to be a nucleon density oscillation that undergoes to drive the sunspot cycle evolution. The beat wavelength λ_{beat} is too long to observe, only the beat period is easy to be observed. This nucleon density oscillation is understood as a new type nuclear reaction in astronomic scale.

In the above calculation, although this seems to be a rough model, there is an obvious correlation between solar radius, solar rotation, solar density, ultimate acceleration and Planck-constant-like constant h.

8. New aspect: coherent width and Easterlies at the equator

Consider an acceleration-roll wave ψ_A at the latitude angle A, it will interfere with its neighbor waves within its coherent width. Because the Earth shell mainly consists of dense matter, their mutual cascade-interference will cause the acceleration roll wave to have the same phase, so that the acceleration roll wave ψ_A should be equal to the $\psi_{equator}$. This conclusion is supported by the spherical symmetry of the Earth density distribution, that is.

$$\text{spherical symmetry: } \rho(r, A, \varphi) = \rho(r) \Rightarrow \psi(r, A, \varphi) = \psi(r)$$

$$\text{or: } \psi_A = \psi_{equator} \tag{29}$$

On the contrary, in the thin atmosphere, the cascade-interference within coherence width can be ignored, so the wind and clouds are widely distributed in the sky on a large scale.

(a)   (b)
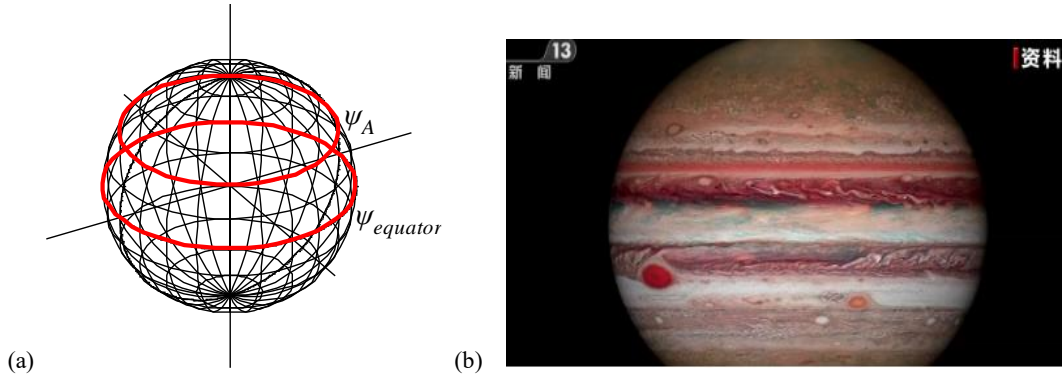
Fig.10   (a) Mutual cascade-interference will lead to the acceleration-roll wave to have the same phase. (b) Jupiter (the photo from News).

```
<Clet2020 Script>// [26]
double beta,H,M,dP[20],D[2000],r,rs,rot,x,y,v1,v2,K1,K2,T1,T2,T,Lamda,V; int i,j,k,N;
int main(){beta=2.961520e10; H=SPEEDC*SPEEDC*SPEEDC/beta;
M=1.9891E30; rs=6.95e8;rot=2*PI/(25.05*24*3600);v1=rot*rs;K1=v1*v1/2;//T1=2*PI*H/K1;
v2=0.7346*sqrt(BOLTZMANN*5700/MP)+0.2485*sqrt(BOLTZMANN*5700/(MP+MP));
K2=v2*v2/2;T2=2*PI*H/(K2-K1);T=T2/24*3600*365.2422;
Lamda=2*PI*H/(v2-v1);V=Lamda/T2;
SetViewAngle("temp0,theta60,phi-60");
DrawFrame(FRAME_LINE,1,0xafffaf);Overlook("2,1,60", D);
for(i=0;i<180;i+=15) {k=0; K1=0; K2=i;Grid();}
for(i=0;i<180;i+=15) {k=1; K1=i; K2=0;Grid();}
//TextAt(10,10,"v1=%d, v2=%d, T=%.2f y, λ=%e, V=%d",v1,v2,T, Lamda,V);
SetPen(3,0xff0000); k=1; K1=60; K2=0;Grid();K1=90; K2=0; Grid();
//SetPen(3,0x4f4fff); k=1; K1=55; K2=0;Grid();K1=65; K2=0; Grid();
TextHang(40,40,50,"#ifψ#sdA#t"); TextHang(50,40,0,"#ifψ#sdequator#t");
}
Grid(){N=50; K1*=PI/180; K2*=PI/180;   r=60;
if(k==0) {v1=2*PI/N; v2=0;} else {v1=0; v2=2*PI/N;}
for(j=0;j<=N;j+=1){ k=j+j+j;
D[k]=r*sin(K1)*cos(K2);D[k+1]=r*sin(K1)*sin(K2); D[k+2]=r*cos(K1);
K1+=v1;K2+=v2; }Plot("POLYGON,0,50, XYZ,10",D);
}#v07=?>A
```

Through the coherent width concept, considering the interference between the air ψ_A at the latitude angle A and the shell ψ_{shell} at the same latitude, they are

$$\psi(r, A) = \psi_{air}(r, A) + C\psi_{shell}(r, A) = \psi_{air}(r, A) + C\psi_{shell\_equator}(r)$$

$$T_{beat} \simeq \frac{4\pi c^3}{\beta\left(v_{shell\_equator}^2 - v_{air}^2\right)} \tag{30}$$

$$v_{shell\_equator} = \omega r$$

$$v_{air} = \omega r \cos(A) + v_{wind} + v_{sun\_effect}$$

where C represents the couple constant which relates to their distance and mass fractions, their interference leads to a beat phenomenon. The positive wind denotes the direction from west to east. The air subjects to the solar radiation which enforces the beat oscillation to run at the period T_{beat}=1 (year) at the latitude angle A=-23.5°N ~ 23.5°N due to the tilt of the Earth axis with respect to the Earth orbital plan. In the northern hemisphere the mean latitude angle A=12°N subjects to the main solar radiation activity, so that at the latitude angle A=12°N location with a wind speed of zero, where the constructive interference condition is satisfied, the beat formula can be used to determine that v_{sun_effect} =-85(m/s). Therefore, we finally decide

$$v_{sun\_effect} = -85\cos(A-12°) \quad .$$ (31)

Near the latitude angle A=12°N location, it is not easy to maintain the constructive interference condition for these waves. The wind required for maintaining the beat T_{beat}=1 (year) near the latitude angle A=12°N is calculated out as shown in Fig.11(b) (blue line), this wind will be destroyed by destructive interference waves at higher latitudes. But, the wind will arise up again at next locations where the waves satisfy the constructive interference condition: at A=48°N location where beat T_{beat}=0.5 (year) and at A=77°N location where beat T_{beat}=0.37 (year) which is the shortest period that the Earth can get within the artic regions. Connecting all characteristic points in Fig.11(a) we obtain the predicted wind-curve over the northern hemisphere; this prediction agrees well with the experimental observations as shown in Fig.12.
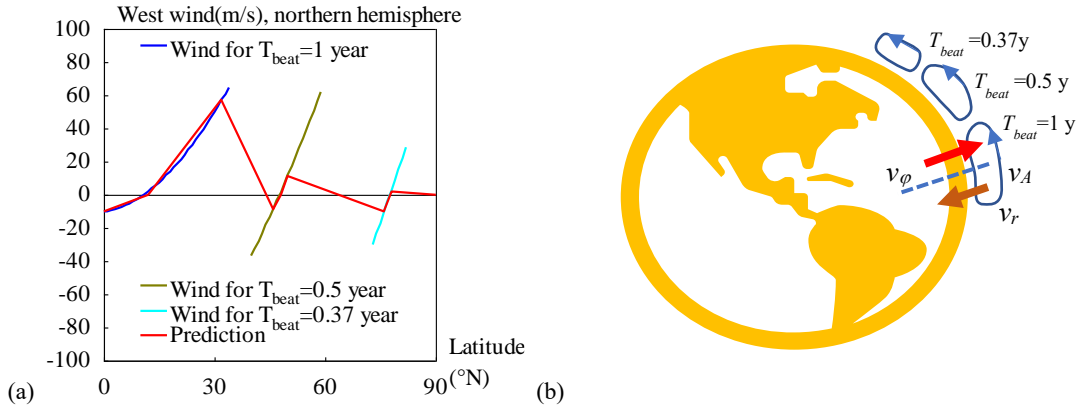

(a)　　　　　　　　　　　　　　　　　　　　　　　　　(b)

Fig.11　　(a) Calculation of west wind in the northern hemisphere. (b) Atmospheric circulation in the northern hemisphere.

```
<Clet2020 Script>// [26]
double beta,H,M,N,r,rc, rs,rot,v1,v2,K1,K2,Year,T,Lamda,V,a,b,w,D[500]; int i, j, k, R;
int main(){beta=1.377075e+14; H=SPEEDC*SPEEDC*SPEEDC/beta;
M=5.97237e24; rs=6.371e6; rot=2*PI/(24*3600); Year=24*3600*365.2422;
SetAxis(X_AXIS,0,0,90,"Latitude#n(°N);0;30;60;90;");
SetAxis(Y_AXIS,-100,-100,100,"West wind(m/s), northern hemisphere;-100;-80;-60;-40;-20;0;20;40;60;80;100;");
DrawFrame(FRAME_BOX,1,0xafffaf);Polyline(2,"0,0,90,0");
T=Year; j=35;for(i=0;i<j;i+=1) {k=i;Wind();D[i+i]=k;D[i+i+1]=V;}
SetPen(2,0xff); Polyline(j,D,10,90,"Wind for T#sdbeat#t=1 year");
T=Year/2; j=20;for(i=0;i<j;i+=1) {k=i+40;Wind();D[i+i]=k;D[i+i+1]=V;}
SetPen(2,0x80ff00); Polyline(j,D,10,-55,"Wind for T#sdbeat#t=0.5 year");
T=0.37*Year; j=10;for(i=0;i<j;i+=1) {k=i+73;Wind();D[i+i]=k;D[i+i+1]=V;}
SetPen(2,0xffff); Polyline(j,D,10,-70,"Wind for T#sdbeat#t=0.37 year");
SetPen(2,0xff0000); Polyline(9,"0,-10,12,0,32,57,46,-8.8,48,0,50,11,76,-10,78,2,90,0,",10,-85,"Prediction");
}
Wind(){ a=k*PI/180;b=(k-12)*PI/180;w=-85*cos(b);
v1=rot*rs*cos(a); v2=rot*rs; K2=v2*v2/2;
K1=K2-2*PI*H/T; V=sqrt(K1+K1); V-=v1+w;
Lamda=2*PI*H/(v2-v1-w);N=Lamda/2*PI*rs*cos(a)*365.2422;
ClipJob(APPEND,"k=%d, v1=%d, wind=%.2f,   T=%.2f y, N=%.2f, V=%.2f",k,v1, V, T/Year, N,Lamda/T);
}#v07=?>A
```

For further improvement of precision, the wind required by the constructive interference

condition should be understood as a magnitude, it can be resolved into three components in the spherical coordinates (r, A, φ) as

$$v_{wind}^2 = v_r^2 + v_A^2 + v_\varphi^2 \quad . \tag{32}$$

According to the energy equipartition theorem in thermodynamics, approximately we have the average estimation

$$<v_r^2> = <v_A^2> = <v_\varphi^2> = \frac{1}{3} v_{wind}^2 \quad . \tag{33}$$

Thus, the wind vectors around the northern hemisphere of the Earth are plotted in Fig.11(b), the atmospheric circulation consists of three cells: Hadley cell, Ferrel cell and artic cell.
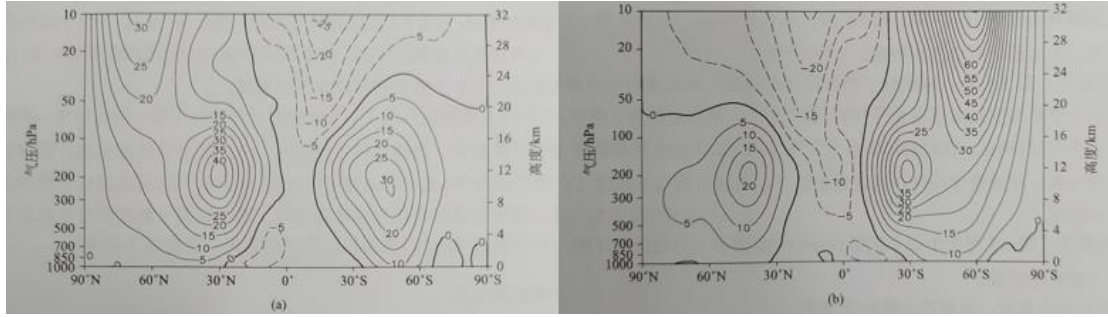

Fig.12   NCEP/NCAR data, mean west winds over 40 years (1958~1997) [36]. (a) in winter; (b) in summer.

The beat T_{beat}=0.5 (year) emits season winds; the shortest beat T_{beat}=0.37 (year) has a beat wavelength too long to be confined in the artic regions so that it escapes from the north pole toward the equator, so recognized as the planet-scale waves or Rossby waves.

Since the acceleration-roll wave of the air interferes with the acceleration-roll wave of the equatorial shell, the easterlies at the equator has a magnitude of about 10 m/s. The trade winds or easterlies are the permanent east-to-west prevailing winds that flow in the Earth's equatorial region. The trade winds blow mainly from the northeast in the Northern Hemisphere and from the southeast in the Southern Hemisphere, strengthening during the winter and when the Arctic oscillation is in its warm phase. Trade winds have been used by captains of sailing ships to cross the world's oceans for centuries. The driving force of atmospheric circulation is the uneven distribution of solar heating across the earth, which is greatest near the equator and least at the poles. This air rises to the tropopause, about 10–15 kilometers above sea level, where the air is no longer buoyant [33].

Consider an funny issue, as we have known that v_{sun_effect} =-85(m/s) near the equator, imagine if nuclear wars happen on the Earth to stop the solar radiation to the Earth surface, then the equatorial wind on the Earth surface will simply reach to 95 (m/s), like the winds on the surfaces of the Jupiter and Saturn [28], this will totally change the global climate mode, killed all dinosaurs by strong winds. Thinking about the Mars, Jupiter and Saturn that gain very weak solar radiation, there are at least 100 (m/s) strong winds on their surfaces, as shown in Fig.10(b). It tells us how important is the easterly 10 (m/s) at the equator for us, how important is the air pollution for us. Have you ever gotten an experience: the more serious the air pollution, the stronger the wind? This section helps us understand how to.

9. Pregnancy of tropical cyclones

A tropical cyclone is a rapidly rotating storm system characterized by a low-pressure center, a closed low-level atmospheric circulation, strong winds, and a spiral arrangement of thunderstorms that produce heavy rain and squalls. Tropical cyclones on either side of the Equator generally have their origins in several tropical cyclone basins, as shown in Fig.13. The Northwest Pacific Ocean is the most active basin on the planet, accounting for one-third of all tropical cyclone activity. Warm sea surface temperatures are required in order for tropical cyclones to form and strengthen. The commonly-accepted minimum temperature range for this to occur is 26–27 °C [37,38].

(a)   (b)
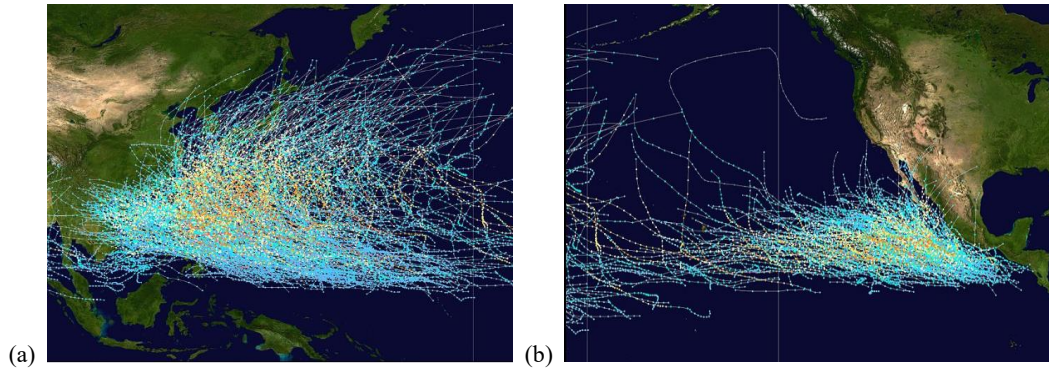
Fig.13   (a) Tracks of all tropical cyclones in the northwestern Pacific Ocean between 1980 and 2005.[39]. (b) Tracks of all tropical cyclones in the northern Pacific Ocean east of the International Date Line between 1980 and 2005.[39]

The latitude $A=12°N$ is called as the first constructive interference line sandwiched between easterlies and westerlies, where the shear action of the winds will produce a lot of vortexes if the winds are disturbed by vapors at higher altitudes. The pregnancy of a tropical cyclone needs three steps, as shown in Fig.14.

(a)   (b)

Fig.14   (a)Three steps of the pregnancy of tropic cyclone. (b) The simulation of cyclone's constructive interference ring.

Step1, during summer, the richer vapor at higher altitudes over the warm sea surface dramatically absorbs the solar radiation and releases the v_{sun_effect} =-85(m/s) into the air at lower altitudes; consequently, the strengthen easterlies make a distortion of the first constructive

18

interference line, as shown in Fig.14(a).
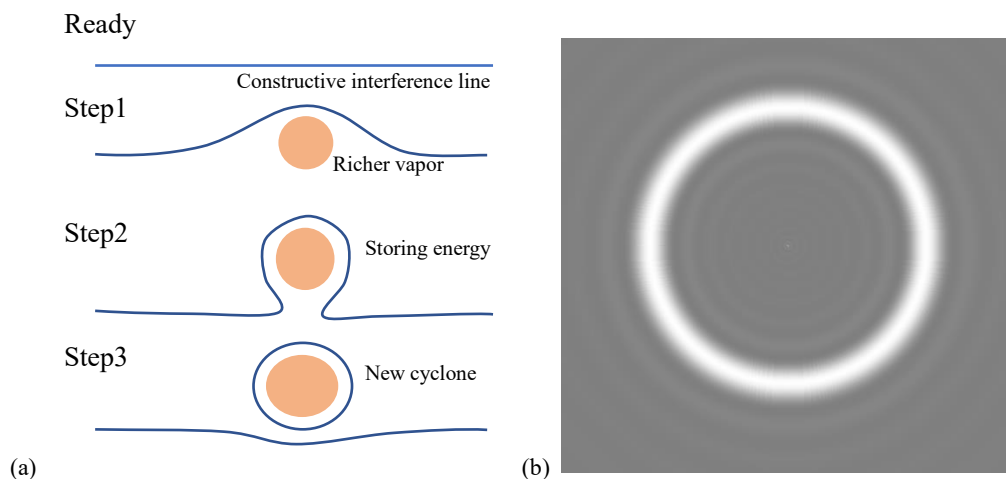
Step2, day by day, the distortion develops to an extent that it is going to separate from the normal the first constructive interference line, as shown in Fig.14(a).

Step3, finally, the distorted constructive interference line grows up to become an isolated ring which is recognized as a new tropical cyclone, as shown in Fig.14(a), similar to Fig.10(b) there is a large vertex on the surface of the Jupiter.

The pregnancy of tropical cyclone tends to develop at the latitude $A=12°N$, it is a relativistic quantum mechanical effect that cannot be settled by the classical fluid mechanics. Recalling that the latitude $A=12°N$ represents the mean latitude angle which subjects to the main solar radiation activity in the northern hemisphere, actually the solar radiation varies its shine within the latitude angle $A=-23.5°N \sim 23.5°N$ due to the tilt of the Earth axis with respect to the Earth orbital plan, therefore actual pregnancy latitude of tropical cyclone occurs among latitude angle $A=-23.5°N \sim 23.5°N$, this result agrees well with the experimental records.

In Fig.11(a), there are the second, the third, …, constructive interference lines to bear the pregnancy of cyclone, hurricane, typhoon, storm, tornado. Without these flexible constructive interference lines, it is difficult for classical physics to say that some disturbances would somehow support the persistence of the vortexes.

When the constructive interference ring of a newly born cyclone forms, its wavelength will adapt to the ring size as

$$\frac{1}{hM_{cyclone}} \oint_L v_l dl = 2\pi n; \quad n = 1, 2, ...$$
$$\psi = \exp(\frac{i}{hM_{cyclone}} \int_0^x (u_1 dx_1 + u_2 dx_2 + u_3 dx_3 + u_4 dx_4))$$

$$(34)$$

where the mass M represents the overall mass of the new cyclone, the constant h is the Planck-constant-like constant determined by experimental observations. The air molecules of the ring are under the control of their acceleration-roll waves whose coherent length is so long that the waves have to overlap as

$$\psi(r) = 1 + e^{i\delta} + e^{i2\delta} + ... + e^{i(N-1)\delta} = \frac{1 - \exp(iN\delta)}{1 - \exp(i\delta)}$$
$$\delta(r) = \frac{1}{hM_{cyclone}} \oint_L (v_l) dl$$

$$(35)$$

This formula can be used to calculate the distribution of the cyclone's nucleon density. The simulation of a cyclone's constructive interference ring is done as shown in Fig.14(b), clearly showing the inner structure of a cyclone. The spin of cyclone was studied in Ref. [28]. Don't underestimate the profound role of the Planck-constant-like constant in cyclone structure; without it, all return back to the classical fluid mechanics.

10. The El Niño Oscillation in the Earth ocean

This section discusses the sea beat phenomenon which arises from the interference between the oceans and the atmospheric circulation near the equator within their coherent width of their acceleration-roll waves, they are given by.

$$\psi = \psi_{sea}(r) + C\psi_{air}(r)$$

$$T_{beat} \simeq \frac{4\pi c^3}{\beta\left(v_{sea}{}^2 - v_{air}{}^2\right)}; \quad v_{sea} = \omega r; \quad v_{air} = \omega r + v_{wind} \qquad . \qquad (36)$$

where C represents the couple constant which relates to their distance and mass fractions, the solar radiation plays a weak role comparing with its role at higher altitudes so that it is ignored for the sea-air friction problem at the sea level.

As a simplest sea-air friction model, regarding the ocean as a static massive matter with the earth self-rotation speed $v_{sea}=\omega r$=463m/s at the equator, approximately, the mean speed of the atmospheric circulation at the equator is v_{air}= v_{sea} -10m/s, see previous section regardless the solar radiation v_{sun_effect}, then their interference gives out their beat period as

$$T_{beat} \simeq \frac{4\pi c^3}{\beta\left(v_{see}{}^2 - v_{air}{}^2\right)} = 8.5\,(years) \quad . \qquad (37)$$
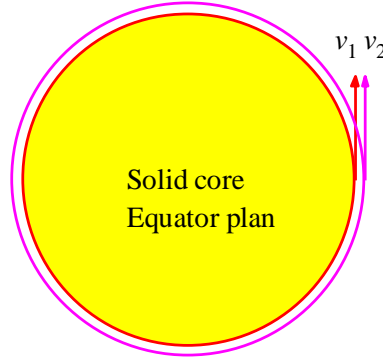

Fig.15   Illustration of overlapping in coherent width direction.

```
<Clet2020 Script>// [26]
double beta,H,M,N,r,rc, rs,rot,v1,v2,K1,K2,T1,T2,T,Lamda,V;
int i, j, k, R,D[50];
int main(){beta=1.377075e+14; H=SPEEDC*SPEEDC*SPEEDC/beta;
M=5.97237e24; rs=6.371e6; rot=2*PI/(24*3600);v1=rot*rs;K1=v1*v1/2;//T1=2*PI*H/K1;
v2=v1-10;//sqrt(M*GRAVITYC/rs);
K2=v2*v2/2;T2=2*PI*H/(K2-K1);T=T2/24*3600*365.2422;
Lamda=2*PI*H/(v2-v1);V=Lamda/T2;
DrawFrame(FRAME_NULL,1,0xafffaf);
//TextAt(10,10,"v1=%d, v2=%d, T=%.2f y, λ=%e, V=%d",v1,v2,T, Lamda,V);
R=80; SetPen(1,0xffff00); D[0]=-R; D[1]=-R; D[2]=R; D[3]=R; Draw("ELLIPSE,1,2,XY,0",D);
SetPen(2,0xff0000); D[0]=-R; D[1]=-R; D[2]=R; D[3]=R;
Draw("ELLIPSE,0,2,XY,0",D);Draw("ARROW,0,2,XY,8","80,0,80,50");
R=85;   SetPen(2,0xff00ff); D[0]=-R; D[1]=-R; D[2]=R; D[3]=R;
Draw("ELLIPSE,0,2,XY,0",D);Draw("ARROW,0,2,XY,8","85,0,85,50");
TextHang(-30,0,0,"Solid core#nEquator plan"); TextHang(70,70,0,"#ifv#sd1#se v#sd2#t");
}#v07=?>A
```

As shown in Fig.15, this beat turns out to be a nucleon density oscillation that undergoes to drive the cycle evolution. It is easy to find that the ocean variation near the equator seems to have a clear positive response to this cycle. El Niño–Southern Oscillation (ENSO) is an irregular periodic variation (4 years—10 years) in winds and sea surface temperatures over the tropical eastern Pacific Ocean, affecting the climate of much of the tropics and subtropics. The warming phase of the sea temperature is known as El Niño and the cooling phase as La Niña. The Southern Oscillation is the accompanying atmospheric component, coupled with the sea temperature change: El Niño is accompanied by high air surface pressure in the tropical western Pacific and La Niña with low air surface pressure there. The two periods last several months each and typically occur every few years with varying intensity per period [33].

11. Global climate change

Detailed estimates of temperature and carbon dioxide levels over the past 800000 years can be made from Antarctic ice samples. Layers of ice have accumulated for more than a million years there. Drilling down through the ice layers, scientists can examine bubbles of gas to find ancient CO_2 levels, and examine the percentage of different oxygen isotopes to estimate the temperature. These detailed measurements are shown in Fig.16. Within this time range, Earth's temperature has gone up and down, with glaciation and CO_2 levels [32].
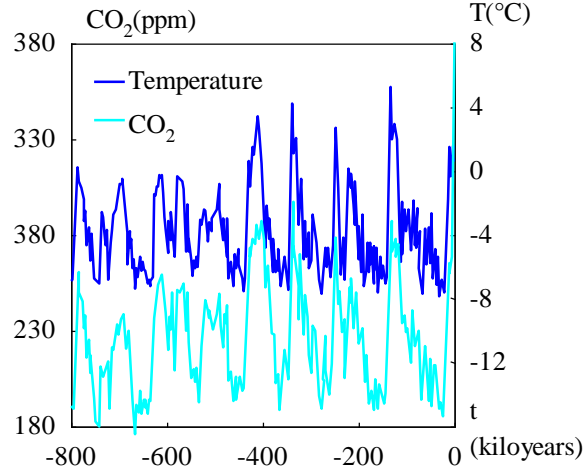

Fig.16   Earth's temperature has gone up and down, with CO_2 levels.

Milankovitch cycles describe the collective effects of changes in the Earth's movements on its climate over thousands of years. The term was coined and named after Serbian geophysicist and astronomer Milutin Milankovitch. In the 1920s, he hypothesized that variations in eccentricity, axial tilt, and precession combined to result in cyclical variations in the intra-annual and latitudinal distribution of solar radiation at the Earth's surface, and that this orbital forcing strongly influenced the Earth's climatic patterns. Similar astronomical hypotheses had been advanced in the 19th century by Joseph Adhemar, James Croll, and others, but verification was difficult because there was no reliably dated evidence in that time, and because it was unclear which periods were important. In recent years, materials on Earth that have been unchanged for millennia (obtained via ice, rock, and deep ocean sediment cores) have been studied to indicate the history of Earth's climate. Although broadly consistent with the Milankovitch hypothesis, a number of specific observations are not explained by the hypothesis.

The Earth self-rotation ω represents the angular speed of the Earth solid core, the angular speed ω_{air} of the atmosphere may differ from the core ω a little bit due to CO_2 impurity. Considering the constancy of angular momentum of the air layer, the difference is estimated by

$$J = m\omega r^2 \quad \Rightarrow \quad \frac{\Delta\omega_{air}}{\omega_{air}} = -\frac{\Delta\rho_{air}}{\rho_{air}} \approx -\frac{\Delta\rho_{CO2}}{\rho_{air}} \quad . \tag{38}$$

$$\Delta\rho_{CO2} = \rho_{CO2}(t) - \rho_{idle}$$

where ρ_{idle} denotes the CO_2 amount that does not contribute to the rotation variation $\Delta\omega$ because its impulse has been absorbed by the Earth solid core for a long time, the ρ_{idle} is about 40ppm in this calculation. The interference takes place between the air acceleration-roll wave and the ground acceleration-roll wave within their coherent width, as shown in Fig.17(a), they are

$$\psi = \psi_{air} + C\psi_{ground}$$

$$\psi_{air} = \exp[\frac{i\beta}{c^3}\int_L (v_1 dl + \frac{-c^2}{\sqrt{1-v_1^2/c^2}}dt)] \quad . \tag{39}$$

$$\psi_{ground} = \exp[\frac{i\beta}{c^3}\int_L (v_2 dl + \frac{-c^2}{\sqrt{1-v_2^2/c^2}}dt)]$$

Where C is the couple constant which relates to their distance and mass fractions, their interference in coherent width direction leads to a beat phenomenon at the radius r location. Over the past 800000 years, the mean CO_2 density in the air is about 220ppm, it is easy to calculate out the beat period of CO_2 density, to be the remarkable 100.6 kiloyears

$$T_{beat} \simeq \frac{4\pi c^3}{\beta(v_2^2 - v_1^2)} = 100604(years) \quad . \tag{40}$$

$$v_1 = (\omega + \Delta\omega_{air})r; \quad v_2 = \omega r$$

Thus, the couple constant C=0.136, the CO_2 density is given by

$$\rho_{CO2}^2 = \rho_{mean\_CO2}^2 + C^2\rho_{mean\_CO2}^2 + 2C\rho_{mean\_CO2}^2 \cos(\frac{2\pi}{T_{beat}}t + \varphi_0) \quad . \tag{41}$$

This result agrees well with the Antarctic ice measurements, as shown in Fig.17(b). The beat wavelength λ_{beat} is too long to observe, only the beat period is easy to be observed.
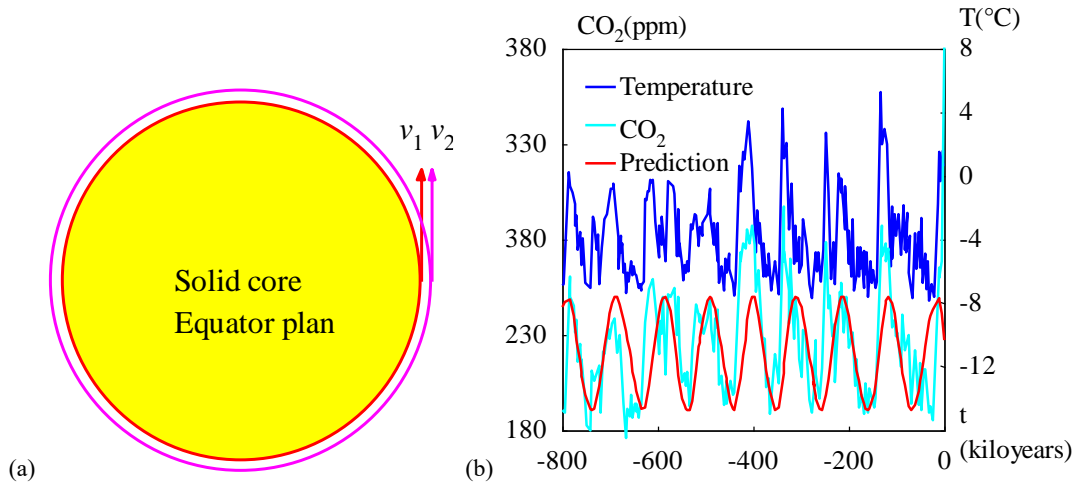

Fig.17   Earth's temperature has gone up and down, with CO_2 levels.

```
<Clet2020 Script>// [26]
double beta,H,M,N,r,rc, rs, a, y, rot,v1,v2,K1,K2,T1,T2,Lamda,V;
int i, j, k, R,D[50];
int main(){beta=1.377075e+14; H=SPEEDC*SPEEDC*SPEEDC/beta;
M=5.97237e24; rs=6.378e6; rot=2*PI/(24*3600);v1=rot*rs;y=1.8e-6;
v2=v1*(1-y);a=(v1*v1-v2*v2)/(2*H); T1=2*PI/a; T2=24*3600*365.2422;
Lamda=2*PI*H/(v2-v1);V=Lamda/T2;
DrawFrame(FRAME_NULL,1,0xafffaf);
//TextAt(10,10,"v1=%d, v2=%d, T=%.2f y, λ=%e,#nV=%d",v1,v2,T1/T2, Lamda,V);
R=80; SetPen(1,0xffff00); D[0]=-R; D[1]=-R; D[2]=R; D[3]=R; Draw("ELLIPSE,1,2,XY,0",D);
SetPen(2,0xff0000); Draw("ELLIPSE,0,2,XY,0",D);Draw("ARROW,0,2,XY,8","80,0,80,50");
R=85;   SetPen(2,0xff00ff); D[0]=-R; D[1]=-R; D[2]=R; D[3]=R;
Draw("ELLIPSE,0,2,XY,0",D);Draw("ARROW,0,2,XY,8","85,0,85,50");
TextHang(-30,0,0,"Solid core#nEquator plan"); TextHang(70,70,0,"#ifv#sd1#se v#sd2#t");
}#v07=?>A


<Clet2020 Script>// [26]
double
D_T[426]={800.00,255.80,795.30,256.38,784.73,315.28,782.38,307.70,777.68,304.20,772.98,298.37,771.81,287.29,769.46,292.
```

22

54,765.93,274.46,762.41,283.79,758.88,266.30,755.36,280.29,750.66,256.97,740.09,254.64,735.39,291.37,730.69,289.04,728.3
4,280.87,725.99,274.46,723.64,282.04,720.12,256.38,715.42,275.63,713.07,282.62,710.72,290.20,706.02,293.12,697.80,306.53,
693.10,306.53,691.92,308.86,681.35,280.87,680.18,264.55,676.65,281.46,675.48,273.29,674.30,277.38,670.78,262.22,668.43,2
66.88,666.08,254.64,666.08,251.72,662.56,262.22,659.03,257.55,654.33,268.05,651.98,261.05,648.46,265.71,647.28,261.63,64
3.76,261.05,639.06,254.05,636.71,256.38,633.19,252.89,632.01,255.80,628.49,257.55,624.96,301.28,621.44,300.12,619.09,304.
78,617.91,304.78,614.39,311.20,612.04,309.45,608.52,311.20,606.17,301.87,603.82,289.04,600.29,282.62,596.77,270.38,595.5
9,286.71,589.72,276.79,589.72,291.95,582.67,268.05,576.80,310.03,567.40,307.70,565.05,303.62,559.18,270.96,556.83,295.45,
552.13,270.96,552.13,277.96,548.60,266.88,546.26,258.13,542.73,266.30,540.38,262.22,536.86,268.63,534.51,262.80,528.63,2
87.87,527.46,284.96,521.59,293.12,518.06,292.54,513.36,277.96,512.19,276.21,509.84,286.12,506.31,281.46,505.14,288.45,49
3.39,293.12,489.87,306.53,488.69,293.12,480.47,276.79,480.47,288.45,473.42,268.05,474.60,288.45,471.07,256.97,464.02,265.
71,460.50,252.89,456.98,269.80,453.45,262.22,448.75,272.13,449.93,264.55,441.70,256.97,439.35,250.55,435.83,256.97,427.6
1,318.19,426.43,304.78,420.56,325.77,417.03,321.69,409.99,341.52,406.46,335.10,400.59,317.03,393.54,272.71,390.01,294.87,
386.49,277.38,384.14,288.45,378.27,260.47,377.09,277.96,371.22,260.47,371.22,266.30,367.69,261.05,366.52,272.13,360.65,2
52.89,353.60,268.63,345.37,251.14,337.15,348.51,334.80,322.27,330.10,330.44,324.23,284.96,319.53,308.86,312.48,266.88,31
0.13,287.29,308.96,268.63,303.08,280.87,301.91,262.22,298.38,266.30,294.86,290.20,287.81,275.63,281.94,256.38,276.06,248.
80,273.72,257.55,267.84,273.29,265.49,262.80,263.14,273.29,256.09,257.55,251.40,274.46,246.70,335.69,242.00,304.20,234.9
5,259.30,230.25,278.54,226.73,256.38,219.68,314.11,214.98,304.20,213.80,311.78,209.10,295.45,207.93,284.96,205.58,307.70,
198.53,266.88,197.36,284.37,193.83,260.47,191.48,290.20,189.13,257.55,187.96,252.89,183.26,261.05,180.91,275.63,176.21,2
60.47,175.04,275.63,173.86,264.55,172.69,273.29,167.99,254.05,165.64,273.88,165.64,261.05,160.94,273.29,158.59,249.97,15
3.89,268.63,150.37,256.97,148.02,263.97,143.32,254.64,140.97,257.55,131.57,356.68,129.22,329.85,124.52,337.43,119.82,329.
85,112.78,282.04,111.60,265.71,108.08,297.20,106.90,269.80,103.38,293.12,99.85,281.46,95.15,293.12,89.28,271.55,83.41,297.
78,81.06,274.46,76.36,293.70,77.53,273.29,71.66,281.46,72.83,262.22,65.79,248.80,58.74,283.21,56.39,264.55,52.86,283.79,48
.16,265.13,46.99,290.79,44.64,256.97,39.94,272.13,35.24,253.47,32.89,268.05,29.37,247.64,24.67,256.38,18.80,249.97,12.92,2
98.37,9.40,325.77,5.87,310.61,2.35,326.36,1.17,318.19,1,320,};
double
D_CO2[338]={797.65,190.50,794.13,188.75,783.55,260.47,783.55,249.97,775.33,245.31,771.81,231.31,768.28,237.73,765.93,2
15.57,762.41,224.90,758.88,207.99,757.71,217.32,750.66,194.58,748.31,182.33,740.09,179.42,736.56,210.90,731.86,205.66,72
1.29,213.82,717.77,188.75,713.07,220.82,709.54,219.65,702.50,233.06,698.97,227.81,694.27,235.98,688.40,238.31,683.70,220.
23,677.83,229.56,669.60,193.41,664.90,175.92,661.38,191.08,657.86,187.00,655.51,198.66,650.81,186.41,647.28,193.99,643.7
6,189.91,643.76,193.99,639.06,186.41,636.71,193.99,633.19,192.83,624.96,236.56,616.74,253.47,609.69,259.30,602.64,238.89,
596.77,219.65,593.25,237.14,590.90,230.15,588.55,249.39,583.85,209.15,576.80,251.14,573.27,249.39,565.05,254.05,559.18,2
29.56,555.65,249.39,553.30,223.73,547.43,205.07,543.91,209.74,540.38,203.32,536.86,210.32,533.33,192.24,527.46,221.98,51
8.06,245.89,512.19,240.06,511.01,236.56,509.84,240.64,502.79,230.15,495.74,238.31,489.87,248.80,486.34,232.48,480.47,220.
82,479.30,238.31,475.77,233.64,473.42,242.97,469.90,203.91,466.37,208.57,459.32,192.83,455.80,205.66,454.63,193.99,446.4
0,205.66,440.53,196.66,438.18,199.83,424.08,272.71,424.08,205.07,419.38,277.96,415.86,275.04,411.16,284.96,406.46,277.96,
404.11,282.04,400.59,287.29,397.06,276.79,392.36,252.30,387.67,263.97,379.44,228.40,374.74,227.81,371.22,202.16,366.52,2
06.82,364.17,188.16,352.42,219.65,345.37,204.49,335.98,297.20,333.63,268.63,333.63,273.88,323.05,252.89,323.05,235.39,32
0.70,269.80,314.83,240.64,313.66,227.81,310.13,248.22,304.26,237.14,301.91,217.32,298.38,207.41,294.86,232.48,290.16,229.
56,280.76,195.74,277.24,188.75,271.37,203.91,272.54,204.49,267.84,227.23,266.67,209.15,259.62,196.33,253.74,212.65,246.7
0,278.54,242.00,243.56,239.65,250.55,233.77,228.98,227.90,235.98,227.90,205.07,218.50,252.30,214.98,244.14,214.98,256.97,
209.10,230.73,203.23,249.97,198.53,223.15,190.31,231.31,185.61,203.32,182.09,216.73,178.56,191.66,172.69,198.66,167.99,1
88.16,164.46,204.49,159.77,188.75,155.07,201.57,145.67,191.66,142.14,196.91,130.40,286.71,130.40,270.96,122.17,277.96,12
1.00,268.05,115.12,275.04,108.08,233.64,103.38,237.73,99.85,228.98,96.33,230.73,89.28,213.24,85.76,240.64,82.23,221.40,74.
01,229.56,66.96,193.41,59.91,221.40,52.86,192.83,49.34,214.99,46.99,190.50,42.29,211.49,38.77,211.49,29.37,189.33,27.02,19
2.24,23.49,185.25,10.57,265.13,9.40,259.88,3.52,268.63,-1.17,380.58,};
```
double rs, rot,beta,H,v1,v2, phase, C, gamma, kiloyears,r1,r2;
double x0,y0,x,y,x1,y1,x2,y2,a,b,D[1000]; int i,j;
main(){ rs=6.378e6;beta=1.377075e+14; H=SPEEDC*SPEEDC*SPEEDC/beta;
rot=2*PI/(24*60*60);//angular speed of the Earth
SetAxis(X_AXIS,-800,-800,0,"t#n(kiloyears);-800;-600;-400;-200;0;");
SetAxis(Y_AXIS,180,180,380,"#Y-10CO#sd2#t(ppm);180;230;380;330;380;");
SetAxis(YA_AXIS,-14,0,8,"T(°C); ;-12;-8;-4;0;4;8;");
DrawFrame(FRAME_BOX,1,0xafffaf);j=213;
for(i=0;i<j;i+=1) {D[i+i]=-D_T[i+i];D[i+i+1]=D_T[i+i+1];}
SetPen(2,0x0000ff); Polyline(j,D,-750,360,"Temperature");j=169;
for(i=0;i<j;i+=1) {D[i+i]=-D_CO2[i+i];D[i+i+1]=D_CO2[i+i+1];}
SetPen(2,0x00ffff); Polyline(j,D,-750,340,"CO#sd2#t");
kiloyears=1000*24*3600*365.2422; x0=-800*kiloyears; x1=x0; Predict2();}
Predict1(){ y=1.8e-6; v1=rot*rs;  y0=0.4e-6;
v2=v1*(1-y); a=(v1*v1-v2*v2)/(2*H); r1=2*PI/(a*kiloyears); r2=0;
C=30/220; y1=220; y2=C*y1; j=169; phase=-PI/4;
for(i=0;i<j;i+=1) {x=D_CO2[i+i];x=-x*kiloyears; y=D_CO2[i+i+1]; y*=1e-8; r2+=y;
v2=v1*(1-y+y0);   a=(v1*v1-v2*v2)/(2*H); phase+=a*(x-x1);
a=y1*y1+y2*y2+2*y1*y2*cos(phase); b=sqrt(a);  x1=x;
D[i+i]=-D_CO2[i+i]; D[i+i+1]=b;}
SetPen(2,0xff0000); Polyline(i,D,-750,320,"Prediction");
TextAt(10,10,"v1=%f, v2=%f, #nr1=%e , r2=%e ",v1,v2,r1,r2/j );}
Predict2(){ j=169; gamma=13.16; y0=2.26e-6;
for(i=0;i<j;i+=1) {x=D_CO2[i+i];x=-x*kiloyears; y=D_CO2[i+i+1]; y*=1e-8;
a=-5+273*(gamma*44/28.966-1)*0.00417*(y-y0)/y0; b=330+a*200/22;
D[i+i]=-D_CO2[i+i]; D[i+i+1]=b;}
SetPen(2,0xff0000); Polyline(i,D,-750,320,"Prediction");
}#v07=?>A
```

The global warming mainly arises from CO_2 impurity. The atmosphere pressure is given by

$$p = \int_0^\infty (\rho_{air} + \Delta\rho)gdh = \int_0^\infty (1 + \frac{\Delta\rho}{\rho_{air}})\rho_{air}gdh \quad . \tag{42}$$

Because the ratio of $\Delta\rho/\rho_{air}$ is not a constant, the above integral cannot carry out generally. The higher the altitude, the lower the air density and the greater the ratio. Let n_{air} denotes the air

molecular density whose mean molecular mass is 28.966; n_{CO2} denotes the CO_2 molecular density whose molecular mass is 44. The pressure variation due to the impurity increasement is estimated by

$$\frac{\Delta p}{p} = \gamma \frac{\Delta \rho}{\rho_{air}} = \gamma (\frac{44}{28.966}) \frac{\Delta n_{CO2}}{n_{air}} \quad . \tag{43}$$

The γ constant is named as stack coefficient for the impurity, it will be determined by experiments. The atmosphere temperature is given by

$$p = nkT$$
$$\frac{\Delta T}{T} = \frac{\Delta p}{p} - \frac{\Delta n}{n_{air}} = (\gamma \frac{44}{28.966} - 1)(\frac{n_{CO2}}{n_{air}})(\frac{\Delta n_{CO2}}{n_{CO2}}) \quad . \tag{44}$$

By mole fraction (i.e., by number of molecules), dry air contains 78.08% nitrogen, 20.95% oxygen, 0.93% argon, 0.0417% carbon dioxide, and small amounts of other gases. Air also contains a variable amount of water vapor, on average around 1% at sea level, and 0.4% over the entire atmosphere. After fitting CO_2 density over last 800 000 years, the stack coefficient takes $\gamma=13.16$. Therefore, the global warming is predicted by the above equation as shown in Fig.18, the result agrees well with the observation from ice samples.
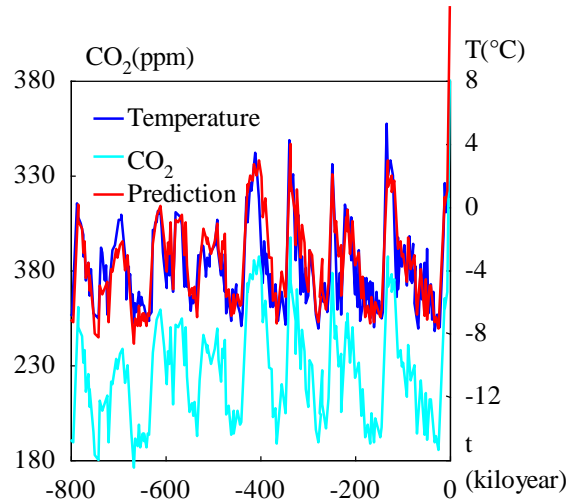

Fig.18   Earth's temperature has gone up and down, with CO_2 levels.

Levels of carbon dioxide have risen by about 30% over the last century, as shown in Fig.19. This increase far exceeds any natural changes over the last 10 million years, so most scientists attribute it to the increased burning of fossil fuels by humans. Human activities such as deforestation, mining coal and metal elements, have also reduced the places where carbon can be stored. Over the same time period, average ocean and air temperatures have increased by about 0.8°C [32], a phenomenon referred to as global warming.

Over the past century, human activities --- various mining, extracting fossil fuels into the atmosphere, airplanes flying in the sky, etc., they all cause a tiny change in the atmosphere. The stack coefficient γ also takes $\gamma=13.16$, this number is obtained from the past 800000 years data. Thus, the global warming is predicted by the above equation as shown in Fig.19, the global temperature has increased about 0.8°C for the past century, this prediction agrees well with the estimation
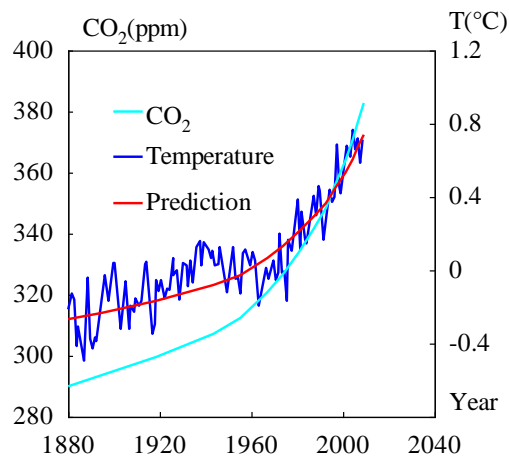
0.8°C/last-century in textbook [32].

Fig. 19　　The prediction of global warming agrees well with the observation for the past century.

<Clet2020 Script> //[26]

```
double
D_T[196]={1880.00,314.94,1881.61,320.36,1882.69,318.19,1883.77,303.01,1884.57,309.52,1887.00,298.40,1888.61,325.24,1889.69,305.45,1890.76,302.20,1891.84,305.72,1892.65,304.64,1896.41,326.05,1897.76,317.65,1900.18,330.12,1900.72,330.12,1903.14,308.70,1905.56,324.16,1906.91,308.70,1907.44,316.02,1909.06,314.40,1909.60,318.46,1911.21,316.30,1912.29,317.65,1913.63,329.85,1914.44,330.66,1916.86,306.81,1917.94,310.33,1918.74,324.43,1919.55,321.17,1920.90,324.70,1921.97,320.63,1922.24,318.73,1923.59,321.99,1924.66,321.45,1926.01,331.75,1926.28,326.33,1927.62,327.95,1928.70,318.19,1930.31,330.39,1931.93,329.58,1932.74,322.80,1933.81,330.93,1934.89,323.61,1936.23,335.54,1937.85,337.44,1938.65,329.31,1939.46,336.90,1941.61,334.73,1942.42,331.75,1943.23,334.19,1944.30,329.31,1945.65,329.85,1946.19,335.27,1949.42,320.63,1952.11,335.27,1953.45,324.97,1954.53,325.51,1955.61,320.09,1956.41,333.37,
1957.49,334.46,1959.64,329.31,1960.72,333.92,1962.06,331.20,1963.68,316.30,1966.64,328.77,1967.71,324.97,1969.60,331.20,1970.67,324.70,1971.75,326.87,1972.56,339.61,1973.63,326.87,1974.71,327.41,1975.78,317.65,1976.32,337.71,1977.67,334.19,1980.63,350.99,1981.43,334.46,1982.24,347.20,1983.59,337.71,1984.39,336.63,1987.35,352.35,1988.70,345.84,1989.51,355.60,1990.31,353.70,1991.93,337.98,1994.62,354.25,1995.70,350.18,1996.77,351.81,1997.85,368.89,1998.65,355.06,1999.46,353.16,2001.61,368.61,2003.23,365.09,2004.57,373.77,2005.38,367.53,2006.46,371.05,2007.53,363.19,2008.61,370.51,};
double
D_CO2[30]={1880.00,290.00,1894.80,293.25,1918.74,299.22,1943.50,307.08,1955.61,312.23,1967.17,320.63,1974.17,326.60,1980.90,333.92,1987.62,341.23,1993.00,348.28,1997.31,356.14,2001.08,363.73,2004.30,370.51,2006.46,376.20,2009.15,382.44,};
double k,y0,x,y,gamma,D[500],a,b;int i,j;
main(){
SetAxis(X_AXIS,1880,1880,2040,"Year;1880;1920;1960;2000;2040;");
SetAxis(Y_AXIS,280,280,400,"#Y-10CO#sd2#t(ppm);280;300;320;340;360;380;400;");
SetAxis(YA_AXIS,-1,0,1,"T(°C); -0.4;0;0.4;0.8;1.2;");
DrawFrame(FRAME_BOX,1,0xafffaf);j=98;
SetPen(2,0x0000ff); Polyline(j,D_T,1900,365,"Temperature");j=15;
SetPen(2,0x00ffff); Polyline(j,D_CO2,1900,380,"CO#sd2#t");
j=15; y0=3e-6; gamma=13.16;
for(i=0;i<j;i+=1) {x=D_CO2[i+i]; y=D_CO2[i+i+1]; y*=1e-8;
a=-0.2+273*(gamma *44/28.966-1)*0.00417*(y-y0)/y0; b=320+a*200/22;
D[i+i]=x; D[i+i+1]=b;}
SetPen(2,0xff0000); Polyline(j,D,1900,350,"Prediction");
}#v07=?>A
```

12. Atmosphere

Above the sea level, air pressure and density decrease with altitude in the atmosphere. The temperature has a more complicated profile with altitude, and may remain relatively constant or even increase with altitude in some regions, as shown in Fig.20(a). Earth's atmosphere can be divided into five main layers: troposphere (0 to 12 km), stratosphere (12 to 50 km), mesosphere (50 to 80 km), thermosphere (80 to 700 km), and exosphere (700 to 10,000 km) [34].

　　The Earth molecules move under the control of their acceleration-roll waves whose coherent length is so long that the waves have to overlap as

$$\psi(r) = 1 + e^{i\delta} + e^{i2\delta} + ... + e^{i(N-1)\delta} = \frac{1-\exp(iN\delta)}{1-\exp(i\delta)}$$

(45)

$$\delta(r) = \frac{\beta}{c^3} \oint_L (v_l)dl = \frac{\beta 2\pi\omega r^2}{c^3}$$

The theoretical Earth radius r_c should appear at the first minimal density that is

$$N\delta = 2\pi \quad \Rightarrow \quad N\frac{\beta 2\pi\omega r_c^2}{c^3} = 2\pi \ .$$

(46)

Let r_s denote the Earth radius at the sea level, the atmosphere height is defined as $h=r_c-r_s$, then we calculate out these parameters from the above equation at the equator as: r_s=6.378000e+6(m), r_c=6.433725e+6(m), h=5.572515e+4(m). Substituting into the density equation, using the core density 5530(kg/m³), we calculate atmospheric density at the sea level to be

$$\rho_0 = 5530(kg/m^3)$$
$$\rho_{r=rs} = \rho_0 \,|\,\psi_{r=rs}\,|^2 = 1.7(kg/m^3)$$

(47)

In a sense, this result agrees well with the real air-vapor density 1.29(kg/m³) at the sea level, this satisfaction indicates that the density equation is a platform qualified for atmosphere study. The atmospheric height is literally h=55.7km, within the range $r<r_c$ in where Earth self-rotation supports the gas speed $v=\omega r$; while in the rang $r> r_c$ the gravity supports space debris speed v=sqrt(GMr) without Earth self-rotation, so that there is a density sudden-change near r_c, as shown in Fig.20(b). In other words, the atmosphere lives in the rang $r_s<r<r_c$; the space debris lives in the rang $r> r_c$.
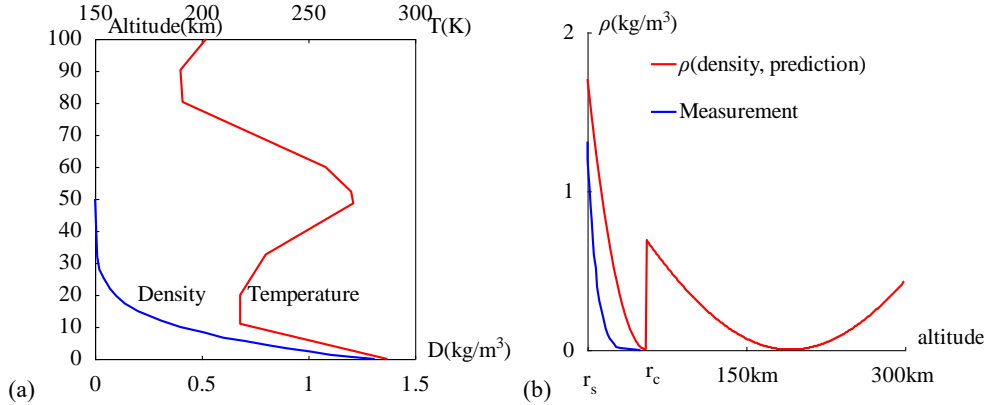

Fig.20   (a) Atmosphere density (blue line) and temperatures (red line) against altitude [32]. (b) Predicted atmosphere density (red line) and real measurement (blue line).

```
<Clet2020 Script> //[26]
double D_D[38]={1.31,0.00,1.20,0.53,1.10,1.32,1.01,2.11,0.90,3.16,0.81,4.21,0.70,5.53,0.60,6.58,0.51,8.16,0.40,9.74,0.31,
11.84,0.20,15.00,0.14,17.11,0.10,19.47,0.07,21.84,0.04,25.26,0.02,27.89,0.01,31.84,0.00,50.00,};
double
D_T[20]={1.37,0.00,0.68,10.79,0.68,20.00,0.80,32.63,1.21,48.42,1.20,52.11,1.08,60.00,0.41,80.26,0.40,90.26,0.52,99.74,};
main(){
SetAxis(X_AXIS,0,0,1.5,"D(kg/m#su3#t);0;0.5;1;1.5;");
SetAxis(XA_AXIS,0,0,1.5,"T(K);150;200;250;300;");
SetAxis(Y_AXIS,0,0,100,"Altitude(km);0;10;20;30;40;50;60;70;80;90;100;");
DrawFrame(FRAME_BOX,1,0xafffaf);
SetPen(2,0x0000ff); Polyline(19,D_D);
SetPen(2,0xff0000); Polyline(10,D_T);
TextHang(0.2,20,0,"Density          Temperature");
}#v07=?>A


<Clet2020 Script>//[26]
int i,j,k,m,n,N,nP[10]; double H,B,M,v_r,r,AU,r_unit,x,y,z,delta,D[10],S[10000];
double rs,rc,rot,a,b,atm_height,p,T,R1,R2,R3; char str[100];
```

```
double D_D[38]={1.31,0.00,1.20,0.53,1.10,1.32,1.01,2.11,0.90,3.16,0.81,4.21,0.70,5.53,0.60,6.58,0.51,8.16,0.40,9.74,0.31,
11.84,0.20,15.00,0.14,17.11,0.10,19.47,0.07,21.84,0.04,25.26,0.02,27.89,0.01,31.84,0.00,50.00,};
main(){k=80;rs=6.378e6; n=0; N=65;
H=1.956611e11;M=5.97237e24;AU=1.496E11;r_unit=1e3;
rot=2*PI/(24*60*60);//angular speed of the Earth
a=N*PI*rot/H;rc=sqrt(PI/a);atm_height=rc-rs;
b=PI/(2*PI*rot*rs*rs/H); R1=rs/r_unit;R2=R1;R3=(rs+3e5)/r_unit;
for(i=R2;i<R3;i+=1) {r=i*r_unit;
if(r<rs+atm_height) delta=2*PI* rot*r*r/H;else delta=2*PI*sqrt(GRAVITYC*M*r)/H;
y=SumJob("SLIT_ADD,@N,@delta",D); y/=(N*N); y*=5530;S[n]=i;S[n+1]=y;n+=2;}
SetAxis(X_AXIS,R1,R1,R3,"altitude; r#sds#t;150km;300km ;");
SetAxis(Y_AXIS,0,0,2,"#ifρ#t(kg/m#su3#t);0;1;2;");DrawFrame(FRAME_SCALE,1,0xafffaf);
x=R1+(R3-R1)/5; SetPen(2,0xff0000) ;Polyline(n/2,S,x,1.8,"#ifρ#ie(density, prediction)");
for(i=0;i<19;i+=1) {S[i+i]=(rs+D_D[i+i+1]*1000)/r_unit;S[i+i+1]=D_D[i+i];}
SetPen(2,0x0000ff) ;Polyline(19,S,x,1.5,"Measurement");
delta=2*PI* rot*rs*rs/H; y=SumJob("SLIT_ADD,@N,@delta",D); y=5530*y/(N*N);
//Format(str,"rc=%e    h=%e    density=%f",rc, atm_height, y); TextAt(10,30,str);
TextHang(rc/r_unit,-0.1,0,"r#sdc#t");
}
#v07=?>A
```

According to this quantum gravity theory, the atmospheric height h=55.7km within the range $r_s<r<r_c$ includes troposphere and stratosphere. The acceleration-roll waves can also be used to explain atmospheric circulation which is the motion of the air through the troposphere in large-scale, and to explain ocean circulation [28].

13. Conclusions

In analogy with the ultimate speed c, there is an ultimate acceleration β, nobody's acceleration can exceed this limit β, in the solar system, β=2.961520e+10(m/s^2). Because this ultimate acceleration is a large number, any effect connecting to β will become easy to test, including quantum gravity tests. In this paper, an approach is put forward to connect the ultimate acceleration with quantum theory, as an application, this relativistic model gives out the sunspot cycle to be 10.38 years due to the ultimate acceleration. The same approach is applied to the Earth El Niño oscillation and global climate change cycle, calculating out the El Niño irregular period to be 8.5 years; calculating out the global climate change cycle to be 100.6 kiloyears which coincides with the Milankovitch cycle; the global temperature has increased about 0.8°C for the past century. In the atmosphere, the more serious the air pollution, the stronger the wind.

References

[1]C. Marletto, and V. Vedral, Gravitationally Induced Entanglement between Two Massive Particles is Sufficient Evidence of Quantum Effects in Gravity, Phys. Rev. Lett., 119, 240402 (2017)

[2]T. Guerreiro, Quantum effects in gravity waves, Classical and Quantum Gravity, 37 (2020) 155001 (13pp).

[3]S. Carlip, D. Chiou, W. Ni, R. Woodard, Quantum Gravity: A Brief History of Ideas and Some Prospects, International Journal of Modern Physics D, V,24,14,2015,1530028. DOI:10.1142/S0218271815300281.

[4]de Broglie, L., CRAS,175(1922):811-813, translated in 2012 by H. C. Shen in Selected works of de Broglie.

[5]de Broglie, Waves and quanta, Nature, 112, 2815(1923): 540.

[6]de Broglie, Recherches sur la théorie des Quanta, translated in 2004 by A. F. Kracklauer as De Broglie, Louis, On the Theory of Quanta. 1925.

[7]NASA, https://solarscience.msfc.nasa.gov/interior.shtml.

[8]NASA, https://nssdc.gsfc.nasa.gov/planetary/factsheet/marsfact.html.

[9]B. Ryden Introduction to Cosmology, Cambridge University Press, 2019, 2nd edition.

[10]D. Valencia, D. D. Sasselov,R. J. O'Connell, Radius and structure models of the first super-earth planet, The Astrophysical Journal, 656:545-551, 2007, February 10.

[11]D. Valencia, D. D. Sasselov,R. J. O'Connell, Detailed models of super-earths: how well can we infer bulk properties? The Astrophysical Journal, 665:1413–1420, 2007 August 20.

[12]T. Guillot, A. P. Showman, Evolution of "51Pegasusb-like" planets, Astronomy & Astrophysics,2002, 385,156-165, DOI: 10.1051/0004-6361:20011624

[13]T. Guillot, A. P. Showman, Atmospheric circulation and tides of "51Pegasusb-like" planets, Astronomy & Astrophysics,2002, 385,166-180, DOI: 10.1051/0004-6361:20020101

[14]L.N. Fletcher,Y.Kaspi,T. Guillot, A.P. Showman, How Well Do We Understand the Belt/Zone Circulation of Giant Planet Atmospheres? Space Sci Rev, 2020,216:30. https://doi.org/10.1007/s11214-019-0631-9

[15]Y. Kaspi, E. Galanti, A.P. Showman, D. J. Stevenson, T. Guillot, L. Iess, S.J. Bolton, Comparison of the Deep Atmospheric Dynamics of Jupiter and Saturn in Light of the Juno and Cassini Gravity Measurements,Space Sci Rev, 2020, 216:84. https://doi.org/10.1007/s11214-020-00705-7

[16]Orbital Debris Program Office, HISTORY OF ON-ORBIT SATELLITE FRAGMENTATIONS, National Aeronautics and Space Administration, 2018, 15 th Edition.

[17]M. Mulrooney, The NASA Liquid Mirror Telescope, Orbital Debris Quarterly News, 2007, April,v11i2,

[18]Orbital Debris Program Office, Chinese Anti-satellite Test Creates Most Severe Orbital Debris Cloud in History, Orbital Debris Quarterly News, 2007, April,v11i2,

[19]A. MANIS, M. MATNEY, A.VAVRIN, D. GATES, J. SEAGO, P. ANZ-MEADOR, Comparison of the NASA ORDEM 3.1 and ESA MASTER-8 Models, Orbital Debris Quarterly News, 2021, Sept,v25i3.

[20]D. Wright, Space debris, Physics today,2007,10,35-40.

[21]TANG Zhi-mei, DING Zong-hua, DAI Lian-dong, WU Jian, XU Zheng-wen, "The Statistics Analysis of Space Debris in Beam Parking Model in 78° North Latitude Regions," Space Debris Research, 2017, 17,3, 1-7.

[22]TANG Zhimei DlNG, Zonghua, YANG Song, DAI Liandong, XU Zhengwen, WU Jian The statistics analysis 0f space debris in beam parking model based On the Arctic 500 MHz incoherent scattering radar, CHINESE JOURNAL 0F RADIO SCIENCE, 2018, 25,5, 537-542

[23]TANG Zhimei，DING, Zonghua，DAI Liandong，WU Jian，XU Zhengwen, Comparative analysis of space debris gaze detection based on the two incoherent scattering radars located at 69N and 78N, Chin．J．Space Sci, 2018 38,1, 73-78. DOI:10.11728/cjss2018.01.073

[24]DING Zong-hua, YANG Song, JIANG hai, DAI Lian-dong, TANG Zhi-mei, XU Zheng-wen, WU Jian，The Data Analysis of the Space Debris Observation by the Qujing Incoherent Scatter Radar, Space Debris Research, 2018, 18,1, 12-19.

[25]YANG Song, DING Zonghua, Xu Zhengwe, WU Jian, Statistical analysis on the space posture, distribution, and scattering characteristic of debris by incoherent scattering radar in Qujing, Chinese Journal of Radio science, 2018 33,6 648-654, DOI:10.13443/j.cjors.2017112301

[26]Clet Lab, Clet: a C compiler, https://drive.google.com/file/d/1OjKqANcgZ-9V5 6rgcoMtOu9w4rP49sgN/view?usp=sharing

[27]Huaiyang Cui, Relativistic Matter Wave and Its Explanation to Superconductivity: Based on the Equality Principle, Modern Physics, 10,3(2020)35-52. https://doi.org/10.12677/MP.2020.103005

[28]Huaiyang Cui, Relativistic Matter Wave and Quantum Computer, Amazon Kindle eBook, 2021.

[29]Huaiyang Cui, Evidence of Planck-Constant-Like Constant in Five Planetary Systems and Its Significances, viXra:2204.0133, 2022.

[30]Huaiyang Cui, Approach to enhance quantum gravity effects by ultimate acceleration, viXra:2205.0053, 2022.

[31]N.Cox, Allen's Astrophysical Quantities, Springer-Verlag, 2001, 4th ed..

[32] S. E. Schneider, T. T. Arny, Pathways to Astronomy, McGraw-Hill Education, 2018, 5th ed.

[33] https://en.wikipedia.org/wiki/El_Ni%C3%B1o%E2%80%93Southern_Oscillation

[34] https://en.wikipedia.org/wiki/Atmosphere_of_Earth

[35] WANG Hui, WANG Aimei , LI Wenshan , LUO Jinxin , ZHANG Jianli, ZUO Changsheng, Changes in key indicators of coastal marine climate in China, Marine Science Bulletin, 2021, 23(1):17-34.

[36] Liping Li et al, Introduction to Atmospheric Circulation, 2nd edition, Science Press, 2021,

[37] https://en.wikipedia.org/wiki/Tropical_cyclone

[38] https://en.wikipedia.org/wiki/Tropical_cyclone_basins

[39] (a) https://commons.wikimedia.org/wiki/File:Pacific_typhoon_tracks_1980-2005.jpg#/media/File:Pacific_typhoon_tracks_1980-2005.jpg).   (b) https://commons.wikimedia.org/wiki/File:Pacific_hurricane_tracks_1980-2005.jpg#/media/File:Pacific_hurricane_tracks_1980-2005.jpg.